



Origin of ferruginous coated grains in the Lower Jurassic palustrine limestones of the Pranhita–Godavari Basin, India

Shantanu Datta¹ | Arnab Sain² | Suparna Goswami¹ | Parthasarathi Ghosh¹ | Concepción Arenas Abad³

¹Geological Studies Unit, Indian Statistical Institute, Kolkata, India

²Department of Geology, Presidency University, Kolkata, India

³Department of Earth Sciences, Institute for Research on Environmental Sciences of Aragón (IUCA) and Geotransfer Group, University of Zaragoza, Zaragoza, Spain

Correspondence

Shantanu Datta, Geological Studies Unit, Indian Statistical Institute, 203 Barrackpore Trunk Road, Kolkata, West Bengal 700108, India.
Email: shantanudatta94@gmail.com

Abstract

The formation of calcareous coated grains like ooids and oncoids have been extensively researched. In contrast, the origin and genesis of ferruginous coated grains are less clear. Radically different processes like surficial weathering, hydrothermal exhalation and microbial activity have been advocated for the source of iron and the development of coatings. Modern examples are sparse and from marine environments affected by igneous activity. This study presents the features of ferruginous coated grains found in freshwater lacustrine–palustrine deposits of the Lower Jurassic syn-rift strata of the Pranhita–Godavari Basin, India. The coated grains occur in metre-thick lenticular bodies of nodular limestones enclosed in black mudstones containing plant debris and sulphates (gypsum and baryte). In the nodular limestones, sand-size coated grains, along with chert and quartz grains, float in a micritic groundmass. Angular quartz grains embedded in dark, amorphous haematite–goethite constitute the nuclei of the coated grains. Cortices comprise numerous, thin, wavy laminae of goethite with trapped detrital grains. These coated grains are typically devoid of carbonates, although the outermost part of the cortex is replaced by calcite spars to varying extent. The black mudstone-nodular limestone association occurs in between siliciclastic lacustrine deposits (laminated red and green mudstones) below, and the palustrine limestones-green shale association above. The palustrine limestones contain remains of aquatic organisms, evidence of desiccation, paedogenesis, microbial-mat formation, chert, baryte and gypsum layers. A few decimetre-scale, wedge-shaped, flood-derived cross-bedded sandstones occur locally. Due to the proximity of the depositional area to the marginal fault system of the rift basin and association of the limestones containing coated grains with sub-aerially weathered microbialites, these ferruginous coated grains are ideally poised for a comparative assessment of various hypotheses of solute supply and precipitation. Based on field, microscopic and chemical characteristics, it is possible to conclude that microbially mediated precipitation in

This is an open access article under the terms of the [Creative Commons Attribution](https://creativecommons.org/licenses/by/4.0/) License, which permits use, distribution and reproduction in any medium, provided the original work is properly cited.

© 2024 The Authors. *The Depositional Record* published by John Wiley & Sons Ltd on behalf of International Association of Sedimentologists.

hydrothermal (hot spring)-influenced pools is the most probable origin for these ferruginous coated grains.

KEYWORDS

coated grains, continental rift basin, iron precipitation, Jurassic, lacustrine, wetlands

1 | INTRODUCTION

The term coated grain was coined by Wolf (1960) for carbonate grains having a distinct nucleus around which concentric layers of calcareous matter accumulated, thereby forming a cortical region (Heim, 1916; Lyell, 1855). The term collectively refers to two main groups—ooids and oncoids (Peryt, 1983; Richter, 1983). Such grains appear in the rock record as well as current environments and have been widely investigated for over half a century. As a result, a fair understanding of the mechanism of repeated accumulation and/or encrustation by minerals like aragonite, Mg-calcite and calcite around a non-stationary core has been attained.

On the other hand, in the literature, there are ample reports of grains that have an internal fabric similar to that of calcareous coated grains but have a cortex made up of iron-bearing minerals. These grains are not uncommon in the geological record. They are found in marine and lacustrine strata ranging in age between Proterozoic and Phanerozoic (Di Bella et al., 2019; Ramajo et al., 2002; Reolid & Abad, 2019; Smith et al., 2020; Thorne et al., 2014; Young, 1989; Young & Taylor, 1989). Modern examples, however, are sparse and are from shallow marine environments affected by igneous activity (Di Bella et al., 2019; Heikoop et al., 1996; Sturesson et al., 2000). Due to the similarity in fabric with calcareous coated grains, the ferruginous counterparts are variously called ferruginous ooids, iron ooids or ferruginous coated grains. Unlike their calcareous counterpart, however, the processes involved in the formation of the layered/laminated cortex are not yet fully understood.

A variety of origins have been proposed for the layered cortex by earlier researchers (Thorne et al., 2014; Young & Taylor, 1989). One group suggested mechanisms that can lead to the development of a layered cortex under stationary conditions that is within a deposit. They include: (1) diagenetic replacement of primary calcareous ooids (Kimberley, 1974, 1979, 1980; Sorby, 1856); (2) accretionary replacement similar to the growth of ground-water nodules/concretions (Anand & Paine, 2002; Anand & Verrall, 2011; Murru et al., 2011; Nahon et al., 1980; Reolid et al., 2008); and (3) enrichment of ferruginous material due to the leaching of mobile phases, resulting in the formation of a laminated structure similar to

the boxwork structure in weathering profiles (Reolid & Abad, 2019; Stoops & Marcelino, 2018). The other group considered that the cortex formed while the grain was in a non-stationary condition like that of a calcareous coated grain. They proposed (1) accumulation (read abiogenic) of iron oxide, where volcanogenic and/or hydrothermal processes are responsible both for the supply of iron as well as for the mobility of the grains (Di Bella et al., 2019; Kimberley, 1994), and (2) microbially induced encrustation around non-stationary grains (Chen et al., 2023).

Unlike calcareous coated grains, ferruginous ones are not common in modern environments that are easy to access, so testing the above-mentioned mechanisms remain incomplete. It also confounds the process of interpreting environmental conditions for the geologically ancient ferruginous coated grains.

In summary, in order to derive information regarding the depositional or diagenetic conditions for the formation of ferruginous coated grains, the following questions need to be addressed:

- Does the cortex form in a stationary (diagenetic/paediogenic) or in a non-stationary condition?
- What is the source of iron and how does it reach the site of precipitation?
- Under what bio-geochemical conditions are iron oxides precipitated?

This study presents the field occurrence, microfabric, mineralogical and geochemical properties of ferruginous coated grains that were found in a Lower Jurassic (Sinemurian to Pliensbachian) palustrine deposit in a continental rift basin succession of India. Proximity to active fault systems, sub-aerially weathered microbialites and siliciclastics, and the presence of evaporite minerals make them ideally poised for a comparative assessment of various hypotheses of solute supply and the mechanism of iron accumulation. A model is proposed for the origin of ferruginous coated grains in a continental rift basin setting based on the properties of these grains and the sedimentological features of their host succession. The proposed source of iron and the mechanisms involved in their precipitation can be relevant for other environments, especially marine. Moreover, this model provides an

alternative to the prevalent concept of prolonged chemical leaching in a subaerial condition.

2 | BACKGROUND

2.1 | Geological range and mineralogical varieties of the ferruginous coated grains

Rocks containing ferruginous coated grains are found throughout the stratigraphic record (cf. Brett et al., 2012). In the Precambrian, sedimentary rocks with high amounts of 'iron ooids' are termed granular iron formations (GIFs), and in the Phanerozoic, they are known as oolitic ironstones, where the term 'ironstone' denotes chemical sedimentary rocks having >15% iron, as defined by Kimberley (1978). The Phanerozoic ironstone deposits are typically much smaller in volume than the GIFs (Bekker et al., 2010; Chen et al., 2023).

The cortex of ferruginous coated grains can be composed of various types of iron-bearing minerals, including iron oxide (e.g. haematite and limonite), iron oxyhydroxide (goethite), iron sulphide (pyrite), iron-bearing phyllosilicate (berthierine and chamosite) and iron carbonate (siderite) (Chen et al., 2023; Garcia-Frank et al., 2012; Scholle & Ulmer-Scholle, 2003; Taylor et al., 2002; Young, 1989).

2.2 | Biotic versus abiotic processes

There is long-standing debate regarding the genesis of ferruginous coated grains (Deverin, 1945; Dubois, 1979; Kelley, 1951; Kimberley, 1980; Maynard, 1986; Mellon, 1962a, 1962b; Reolid et al., 2008) as well as oolitic ironstone deposits (Formozova, 1959; Kholodov et al., 2012; Kimberley, 1989, 1994; Krotov, 1951; Maynard, 1983; McGregor et al., 2010; Novoselov et al., 2018; Pettijohn, 1975; Van Houten, 1992). Both biotic (Burkhalter, 1995; Chen et al., 2023; Dahanayake & Krumbein, 1986; Smith et al., 2020) and abiotic (Van Houten & Purucker, 1984) mechanisms have been proposed. Preat et al. (2008) suggested that microbial activity might have played a significant role in the precipitation of iron oxides and hydroxides during the formation of coated grains. On the other hand, the proposed abiotic mechanisms include: (i) replacement of carbonate ooids with iron-rich minerals (Kimberley, 1974, 1979, 1980; Sorby, 1856); (ii) micro-concretionary in situ growth; (iii) formation of iron hydroxide from gel; (iv) mechanical adhesion of clay with subsequent transformation into iron-enriched aggregates; (v) erosion of lateritic soil (Formozova, 1959; Young, 1989); and (vi) development of

pisolitic structures in hydromorphic ferruginous soil like a plinthite (Reolid et al., 2008; Reolid & Abad, 2019).

2.3 | Depositional environments

Ferruginous coated grains can form in various environments: (i) marine (Berendsen et al., 1992; Chauvel & Massa, 1981; Collin et al., 2005; Gygi, 1981; Kimberley, 1979, 1994; Kogbe, 1978; Ramajo et al., 2002); (ii) in the environments of early subaqueous diagenesis or subaerial paedogenesis (Dubois & Icole, 1977; James & Van Houten, 1979; Nahon et al., 1980); (iii) at the site of placer deposition fed by eroding lateritic/plinthitic soils and characterised by reworking of particles (Aurell et al., 1994; Reolid et al., 2008; Siehl & Thein, 1978, 1989); (iv) in shallow marine volcanic settings (Heikoop et al., 1996; Soussi & M'rabet, 1991; Sturesson, 2003; Sturesson et al., 2000); (v) in alluvial settings such as deltaic and lacustrine (Formozova, 1959; Kholodov et al., 2012); and (vi) in terrigenous settings by catagenetic processes (Pavlov, 1989, 1995).

A review of the environmental settings and the various modes of formation of the ferruginous coated grains is given in Thorne et al. (2014), Young (1989) and Young and Taylor (1989).

2.4 | Source of iron

A crucial question related to the formation of ferruginous coated grains and ironstones is the source of iron. The views are quite diverse there as well. It has been suggested that the iron can be supplied either by surficial weathering (i.e. soil formation or chemical alteration of marine sediments) or due to exhalation of deep fluids (i.e. by magmatic devolatilisation or due to ascent of shallower-sourced fluids, like sea water, due to convection) (Kimberley, 1994). In an environment of high terrigenous input, iron solute can be supplied by catagenetic processes that is along with underground waters originating from the compaction and dehydration of pelitic rocks (Pavlov, 1989, 1995). Dreesen (1989) suggested that in the case of the replacement of carbonate ooids with iron, the solute might be sourced from volcanic ash deposits.

Other authors have discussed how the supply of iron to the oceans might have changed over geological time. For example, it has been suggested that the smaller volume of the Phanerozoic oolitic ironstones, compared to the Precambrian GIFs, is due to the fact that the supply of iron has gradually diminished in Phanerozoic seas as a consequence of repeated oxygenation events in the early Palaeozoic (Bekker et al., 2010; Chen et al., 2023; Taylor et al., 2002; Young, 1989). The ironstones forming in

Phanerozoic seas depended mainly on the contributions from terrestrial weathering, volcanic ash deposits and submarine hydrothermal fluids (Chen et al., 2023).

2.5 | Geological setting

Ferruginous coated grains have been found in the Lower Jurassic strata of the Pranhita–Godavari Valley (PGV) Gondwana Basin of India. The basin-fill strata of the PGV Basin are exposed in an NNW–SSE trending linear outcrop belt (400 km long, 75 km wide) in the central Indian states of Telangana, Maharashtra and Andhra Pradesh (Figure 1). The strike of the beds is 150°, and they dip at an angle of 10–12° towards ENE.

The PGV Basin is one of the main Gondwana basins of Peninsular India. Gondwanaland was under a regime of extensional tectonic forces since the Late Palaeozoic, and it finally broke up into smaller landmasses in the Jurassic (Acharyya, 2000; Biswas, 1999, 2003; Chakraborty et al., 2003; Chatterjee & Ghosh, 1970; Mitra, 1987, 1994; Naqvi et al., 1974; Veevers & Tewari, 1995). Initially, in the Late Palaeozoic, a set of interconnected sag basins formed all over Gondwanaland (Biswas, 1999; Casshyap & Tewari, 1991; Veevers & Tewari, 1995). At the beginning of the Triassic Period, in the peninsular part of the Indian landmass, several basins became differentiated, and each of them started evolving independently. The PGV began to evolve as a NNW–SSE-oriented continental rift basin that persisted at least until the early Middle Jurassic. The

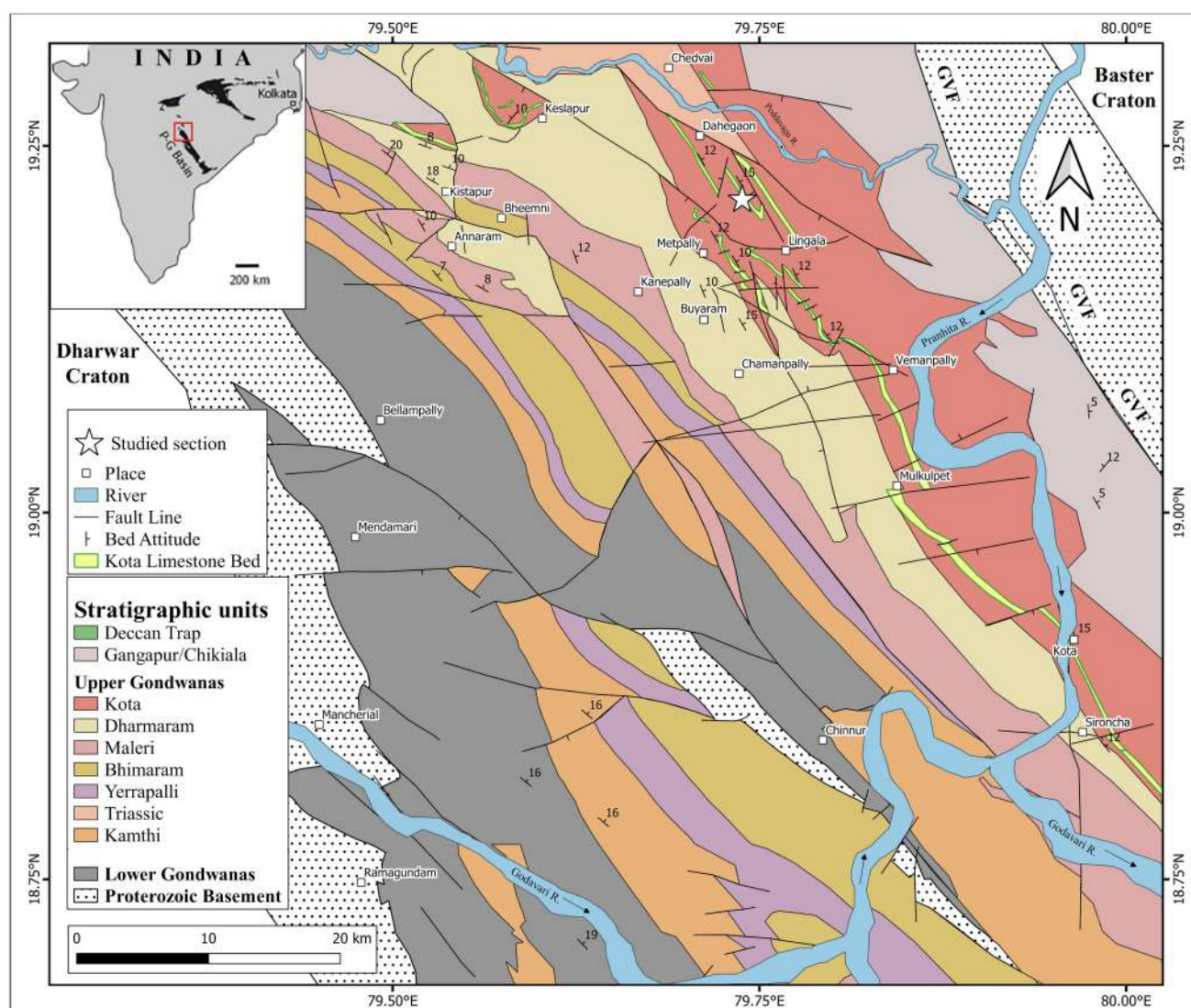


FIGURE 1 The northern part of the exposure belt of the Pranhita–Godavari Gondwana Basin, India (modified after Goswami & Ghosh, 2020; Kutty et al., 1987; Kutty & Sengupta, 1989). Proterozoic basement rocks border the exposure belt in the SW and NE. The Godavari Valley Fault System is marked as GVF. The location of the exposure belt (red box) in the peninsular part of India is given in the inset.

eastern margin of this rectilinear basin is demarcated by the Godavari Valley Fault System (GVF) (Biswas, 2003; Goswami & Ghosh, 2020; Ghosh & Sengupta, 2020), which separates the basin-fill strata from the Archean and Proterozoic basement rocks lying to the east. In the west, these syn-rift strata rest conformably on the pre-rift deposits of the PGV.

At least a 3 km thick pile of sediments had accumulated in this half graben starting from the Triassic until the Middle Jurassic (Bandyopadhyay & Rudra, 1985; Bandyopadhyay & Sengupta, 2006; Goswami & Ghosh, 2020; Kutty et al., 1987; Robinson, 1967; Rudra, 1982; Sengupta, 1970), and these sedimentary rock strata are collectively known as the Upper Gondwanas (Ghosh & Sengupta, 2020; Table 1).

The Upper Gondwanas of the PGV Basin is dominated by siliciclastic deposits of alternating sandstones and mudstones, except for a 20 to 30 m thick limestone-bearing interval that occurs in the middle part of the Kota Formation. This interval is commonly referred to as the Kota Limestone bed. The sedimentological and palaeontological evidence suggest that these syn-rift sediments were deposited mainly in a variety of fluvio-lacustrine environments (Dasgupta et al., 2017, 2022; Goswami & Ghosh 2020; Kutty & Sengupta, 1989).

The Kota Formation conformably overlies the older syn-rift strata, that is the Dharmaram Formation (Upper Norian to Hettangian in age), and underlies the Lower Cretaceous post-rift strata, separated across an unconformity (Ghosh & Sengupta, 2020). The formation is about 550–600 m thick (Goswami et al., 2018; Rudra, 1982). The basal 100 m of the succession comprise red mudstones and sandstones (Rudra, 1982; Rudra & Maulik, 1994). This siliciclastic succession grades upwards to a Kota Limestone bed (20–30 m thick; Goswami et al., 2018; Rudra, 1982). This interval comprises alternating, metre-thick beds of structureless, nodular and laminated limestones, and laminated yellow and greenish black ferruginous mudstones (Figure 2).

A variety of flora and terrestrial fauna, like large fishes, turtles, crocodiles, mammals, dinosaurs, freshwater ostracods, conchostracans and land insects, are found in this interval (Table 1; Bandyopadhyay, 2011; Chatterjee & Roy Choudhury, 1974; Goswami et al., 2018; Goswami & Ghosh, 2020; Jain, 1980; Kutty, 1971; Pascoe, 1959; Sarkar & Chaudhuri, 1992). Based on the fish fossils, the lower siliciclastic part of the Kota Formation has been assigned a Sinemurian age, whereas the Kota limestone bed has been assigned a Toarcian age (Bandyopadhyay & Sengupta, 2006). Based on stratigraphic considerations, Bandyopadhyay and Sengupta (2006) have suggested that the uppermost part of this formation could be Aalenian in age. The dinosaur fauna in the lower part of the Kota

Formation also indicates a Middle Jurassic age (Prasad & Parmar, 2020).

Based on facies analysis, Goswami and Ghosh (2020) suggested that the basal siliciclastic succession of the Kota Formation was deposited in a variety of lake-margin environments (Figure 2). In addition, the overlying Kota Limestone interval preserves the features of palustrine carbonates and microbialites (Goswami et al., 2018; Goswami & Ghosh, 2020, 2021). The carbonate and siliciclastic facies of the Kota Limestone Bed indicate that this interval represents a freshwater carbonate-precipitating wetland system where fine-grained siliciclastics were periodically introduced by sheet-flood processes. The ferruginous sandstones and mudstones overlying the Kota Limestone interval have been ascribed to a fluvial deposit (Rudra & Maulik, 1994). The occurrence of evaporite minerals (gypsum and baryte) at the base of the limestone interval has been ascribed to an increase in aridity after deposition of the basal siliciclastic succession of the Kota Formation under semi-arid conditions (see Goswami, 2021; Goswami & Ghosh, 2021). The ferruginous coated grains described here occur in the uppermost part of the siliciclastic succession below and in the lowermost beds of the Kota Limestone bed above.

3 | MATERIALS AND METHODS

The exposures of the Kota Formation in the northern part of the PGV Basin, bound by latitudes 18°70' N and 19°40' N and longitudes 79°38' E and 80°10' E, were studied in the field. The lithological and sedimentological features were documented in the natural, river-cut sections and along the banks of irrigation canals. Representative samples were collected from each lithological type and sub-type as observed in profile sections. An attempt was made to sample each stratigraphic level in as much detail as practicable. Care was taken to avoid weathered parts while collecting the samples. Lithologs were prepared using the standard methods to document the stratigraphic disposition of the ferruginous coated grain-bearing horizons and other lithofacies in a 50 m thick succession spanning the lower siliciclastic part and the limestone-bearing interval of the Kota Formation.

The microfabric of the ferruginous grains and associated sediments were studied in polished slabs and thin sections under polarising microscopes. A total of 56 samples were studied using both transmitted and reflected illuminations. Panoramic images of the thin sections were collected using DinoLite and Leica DVM6 digital microscopes. Both optical and longwave ultraviolet (432 µm wavelength) illuminations were used.

TABLE 1 Stratigraphy of the Gondwana succession of the Pranhita–Godavari rift basin, central India. The general lithological attributes, faunal records and the age are taken from Bandyopadhyay et al. (2010), Bandyopadhyay and Rudra (1985), Bandyopadhyay and Sengupta (2006), Goswami and Ghosh (2020), Jain et al. (1964), Kutty et al. (1987), Kutty and Sengupta (1989), Ray and Bandyopadhyay (2003).

Formation	Lithologies	Major fossils	Age
Chikiala	Highly ferruginous sandstones and conglomerates		Cretaceous
Gangapur	Coarse gritty sandstones, greyish white to pinkish mudstones with interbedded ferruginous sandstones and concretions	<i>Glattenla</i> , <i>Pagiophylthum</i> , <i>Pilllophylum</i> , <i>Elactoclachus</i>	Lower Cretaceous
Upper Gondwanas			
Kota	Sandstone, siltstone, mudstone and limestone bands	'holosteans', sauropods, sphenodontians, lepidosamirids, crocodylomorphs, cryptodire, 'symmetrodonts'	Lower to Middle Jurassic
Dharmaram	Coarse sandstone and mudstone	Sauropodomorpha, Neotheropoda, sphenosuchians, phytosaurids, aetosaurids	upper Upper Triassic to lower Lower Jurassic
Maleri	Mudstone, fine to medium sandstone and calcirudite	Metoposaurid, chigutisaurids, phytosaurids, rhynchosaurid, prolecerid, aetosaurids, dicynodont, cynodont, basal dinosauroides, sauropodomorpha	lower Upper Triassic (Upper Carnian–Lower Norian)
Bhimaram	Coarse to fine sandstone, ferruginous or calcareous at places and mudstone		upper Middle Triassic (Ladinian)
Yerrapalli	Red and violet mudstone and calcirudite	Capitosaurs, therapsids, cynodont, rhynchosaur, prolacerid, rauiisuchid, erythrosuchid	lower Middle Triassic (Anisian)
Kamthi	Sandstone and siltstone	Brachyopid, therapsid, <i>Glossopteris Flora</i>	Lower Triassic
Lower Gondwanas			
Kundaram	Ferruginous shale, mudstone and sandstone	<i>Endotheodon</i> , <i>Oudenodon</i> , <i>Kingoria</i> , <i>Emydops</i> , <i>Cistecephalus</i> , <i>pristerodon</i> , <i>Captohrinid</i>	upper Upper Permian
Barakar	Sandstone, carbonaceous shale and coal	<i>Glossopteris Flora</i>	lower Upper Permian
Talchir	Tillites, Greenish shale and sandstones		lower Lower Permian
Unconformity			
Proterozoic sedimentary rocks and Archean basement rocks			

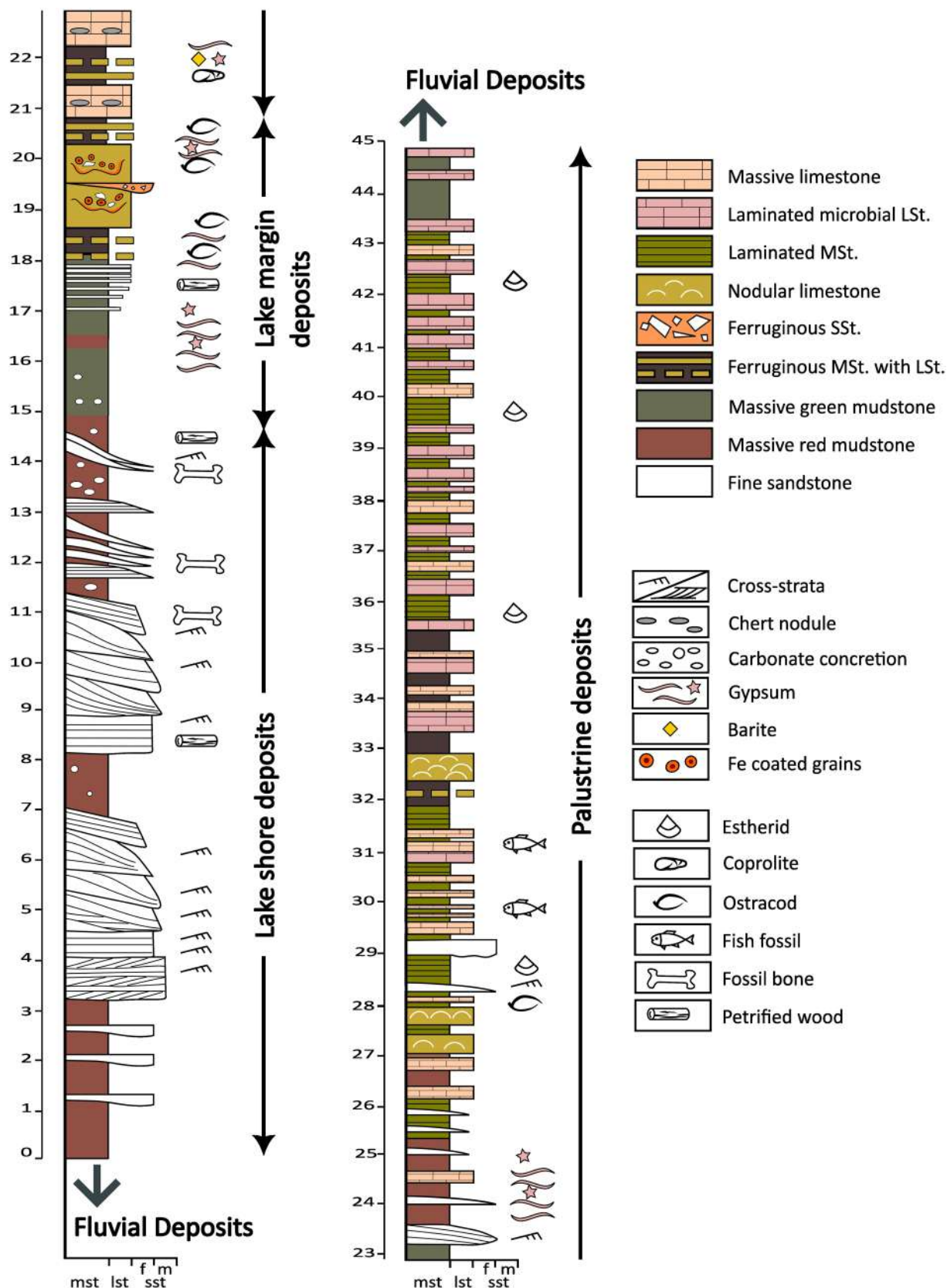


FIGURE 2 Lithological log for the Lower Jurassic part of the succession near the Metpalli village, Telangana, India. The top of the Lower Member of the Kota Formation is at 15 m. The ferruginous coated grains occur in the stratigraphic interval between 18.5 and 20.5 m. The vertical scale is in metres.

Sub-microscopic morphological features were studied using a scanning electron microscope (SEM)—secondary electron (SE) and backscatter electron (BSE) imaging. Elemental compositions were determined from the energy dispersive X-ray (EDX) spectra obtained at 24 points across the nucleus and cortex of two ferruginous grains and their associated sediments. Chips and thin sections coated with platinum were examined by elemental mapping in an environmental SEM (Model: Carl Zeiss EVO 18 Special Edition) equipped with an INCA Energy 250 microanalysis EDX at the Centre for Research in Nanoscience and Nanotechnology (CRNN, University of Calcutta, India). The BSE imaging and EDX analysis were done mostly on carbon-coated samples in a JEOL JSM IT-500 microscope fitted with an EDX system belonging to the Department of Geology, Presidency University, Kolkata, India. Here, the quantitative analyses of the selected minerals were conducted at an accelerating voltage of 20 kV, a probe current of 48 nA and an accumulation time of 15 s.

Mineralogical compositions determined using microscopy were supplemented through X-ray powder diffraction (XRD) analysis and laser Raman spectroscopy. For XRD analysis, the grains were separated from the carbonate matrix using a micro-drill. The residual carbonates were removed by washing the samples with weak organic acid. Air-dried samples were powdered in an agate mortar with a pestle.

One set of powdered samples were analysed in a Bruker AXS (Model No. D8 Advance) XRD in the Department of Central Scientific Services, Indian Association of Cultivation of Science, Kolkata, India, fitted with a Lynxeye super speed detector using Cu-K α radiation ($\lambda = 1.5406 \text{ \AA}$) at 40 kV and 40 mA. The samples were scanned for 2θ values from 5 to 60° with a step size of 0.02056° at a scan speed of 0.04°/2 θ per minute. Another set of samples was analysed in a PANalytical X'Pert-3 Diffractometer (X-ray Mineral Services Ltd., North Wales, UK) fitted with PIXcel 1-D detector using Cu-K α radiation ($\lambda = 1.540598 \text{ \AA}$) at 40 kV and 40 mA with a scan speed of 0.01°/2 θ per minute with 2θ ranging from 4.5 to 75°, with a step size of 0.01291°. The obtained diffractograms were interpreted with the open-source software PROFEX 5.2.0 (Doebelin & Kleeberg, 2015) for phase identification using Rietveld refinement using BGMN and COD databases. Apart from phase identification, the degree of Al³⁺ substitution in the goethite structure was determined from the diffractograms using the method described by Schulze (1984).

The mineralogical study was complemented with laser Raman spectroscopy. The Raman spectra were measured from the uncovered thin sections with a Jobin–Yvon Horiba Triple Raman Spectrometer (Model: T64000), equipped with 1800 grooves/mm gratings, TE-cooled Synapse CCD detector and an open-stage Olympus microscope with

50x objective (M Plan) and numerical apertures of 0.75, housed at the Department of Central Scientific Services, Indian Association of Cultivation of Science, Kolkata, India. The samples were excited with 633 and 532 nm wavelength (red and green, respectively) lasers from the DPSS (Diode Pump Solid State Laser) Nd:YAG laser (Make: Spectra Physics). Raman spectra were obtained for 10 points across the nucleus and cortex of three coated grains using various laser powers. The spectral data were compared with the entries in the RRUFF Project database (Downs, 2006) for mineral identification using CrystalSleuth software version 20 July 2009 (Laetsch & Downs, 2006). From the Raman spectra, the percentage of Al³⁺ substitution in the goethite structure was computed using the method described by Liu et al. (2013).

Quantitative XRD analysis was performed to determine the amounts of clay minerals in the <2 μm size fraction of four mudstone samples. The samples were crushed and dispersed in distilled water. The <2 μm size fraction was then separated by gravity settling of particles in suspension. Oriented aggregates of the <2 μm size fraction were prepared by placing a portion of the suspension onto a glass slide. In order to identify expandable clay minerals, the oriented slides were air-dried and saturated with ethylene glycol. The XRD analysis was performed on a PANalytical X'Pert Pro diffractometer equipped with a Cu X-ray source and an X'Celerator detector and operating under the following conditions: 40 kV and 40 mA; range 3–30°/2 θ ; step size 0.017°/2 θ ; time per step 50.165 sec; fixed divergence slit, angle 0.5 or 0.25°; sample rotation 1 rev/sec. The semi-quantitative amounts of the clay minerals in the <2 μm size fraction were determined based on the area of their basal peaks.

4 | RESULTS

4.1 | Field occurrences and lithological characters

The interval bearing ferruginous coated grains is located between 18.5 and 20.5 m above the base of the succession (Figure 2). It occurs between the siliciclastic lake-margin deposits below and the carbonate-rich lacustrine–palustrine succession above (Figure 3). This interval is characterised by 0.5 to 3 m thick lenticular yellowish-grey limestone bodies enclosed within greenish and reddish-black carbonaceous and ferruginous mudstones (Figure 4A). Apart from the lenticular limestone bodies, a few sheet-like bodies of fine-grained sandstones, tens of centimetres thick, occur in this interval (Figure 3C). The presence of profuse gypsum (rosettes, satin-spar veins and nodular masses) in the mudstones is a characteristic feature of this interval

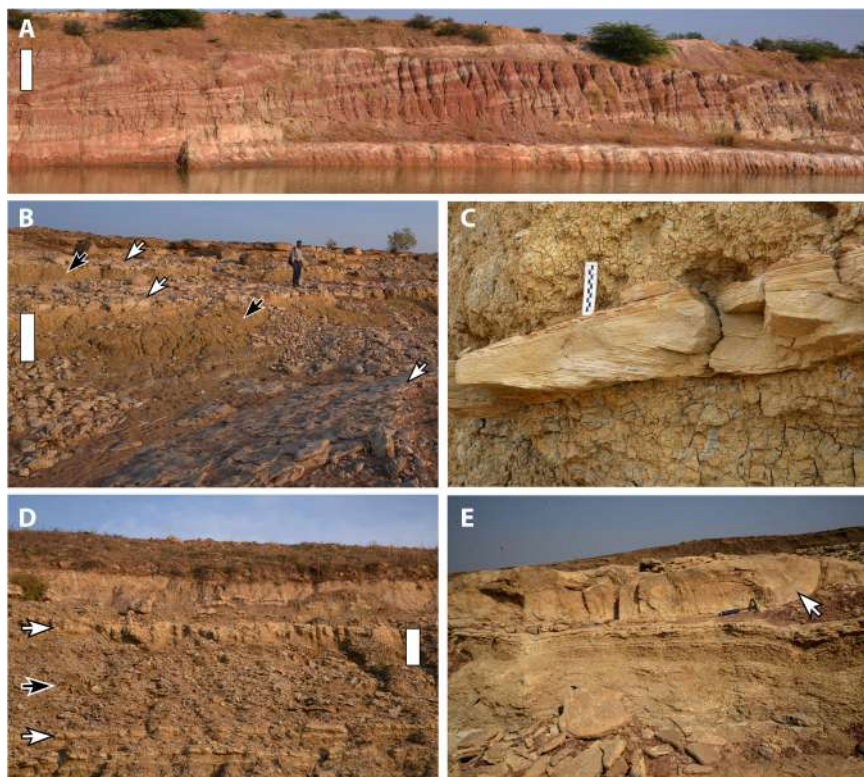


FIGURE 3 (A) Field photograph showing deposits of the siliciclastic lake mouth-bar complexes lying below the interval bearing ferruginous coated grains. The dip of the strata is away from the observer. Scale bar 3 m. (B–E) The exposures of the overlying palustrine deposits; (B) Alternating mudstone (laminated, black arrow) and limestone (laminated and structureless, white arrow) beds. Scale bar 2 m. (C) A sheet-flood deposit enclosed by the paedogenically modified calcareous mudstone. Note the cross-lamination over the slightly concave-up base and horizontal lamination at the flat-shaped top of the sandstone body, as well as the drab haloes in the mudstone. The scale is graduated in centimetres. (D) The basal part of the palustrine succession showing lenticular bodies of structureless limestones (white arrow) in gypsum-bearing mudstones (black arrow). Scale bar 30 cm. (E) Close-up view showing a lenticular microbial limestone body (arrow) overlying laminated mudstones. Hammer for scale.

(Figure 3D). The overlying lacustrine–palustrine succession (20–30 m thick) is characterised by alternations of metre-thick beds of greenish-yellow shale, microbially laminated limestones and structureless/nodular palustrine limestones (Figure 3B,E). See Goswami et al. (2018) and Goswami and Ghosh (2020, 2021) for details.

The lower and the upper contacts of the limestone bodies with the enclosing dark mudstones are gradational. Usually, the upper and the lower parts of the limestone bodies are laminated, and they are made up of dark peloidal micrite containing articulated and disarticulated shells of bivalves oriented parallel to the lamina (Figure 4B). Bioclast (ostracod)-rich and bioclast-poor laminae could be observed at thin-section scale.

The coated grains occur in structureless units in the middle part of the limestone bodies. These structureless units are a few centimetres thick and continue laterally for a few metres. Their boundaries with the underlying and overlying laminated units are gradational. Except for these units, the limestone is generally not ferruginous. In such structureless units, the ferruginous coated grains (1

to 5 mm in diameter) admixed with a few medium sand-sized detrital grains (quartz and chert fragments) float in a groundmass made up of micrite-microspar (Figure 4C). In hand samples, these grains are associated with small-scale contorted surfaces (due to dissolution?) that are lined with iron oxides (Figure 4D). Bioclasts and calcareous coated grains are typically absent.

In some places, the coated grains are very tightly packed (Figure 4C). The grains are in contact with each other, with very little carbonate cement (microspar) between them. These grains are poorly sorted, typically spherical in shape and well rounded. In general, the surface of the grains appears rough and lustreless, with a metallic lustre only visible in minute patches. They are brownish black in hand samples and weakly magnetic. When touched, they appear as a compact and hardened material that does not stain fingers. The streak is dusky yellowish brown (Munsell Colour: 10YR 2/2).

The black ferruginous mudstones enclosing the limestone bodies are characterised by the presence of ultrathin lamination defined by variations in carbonaceous matter

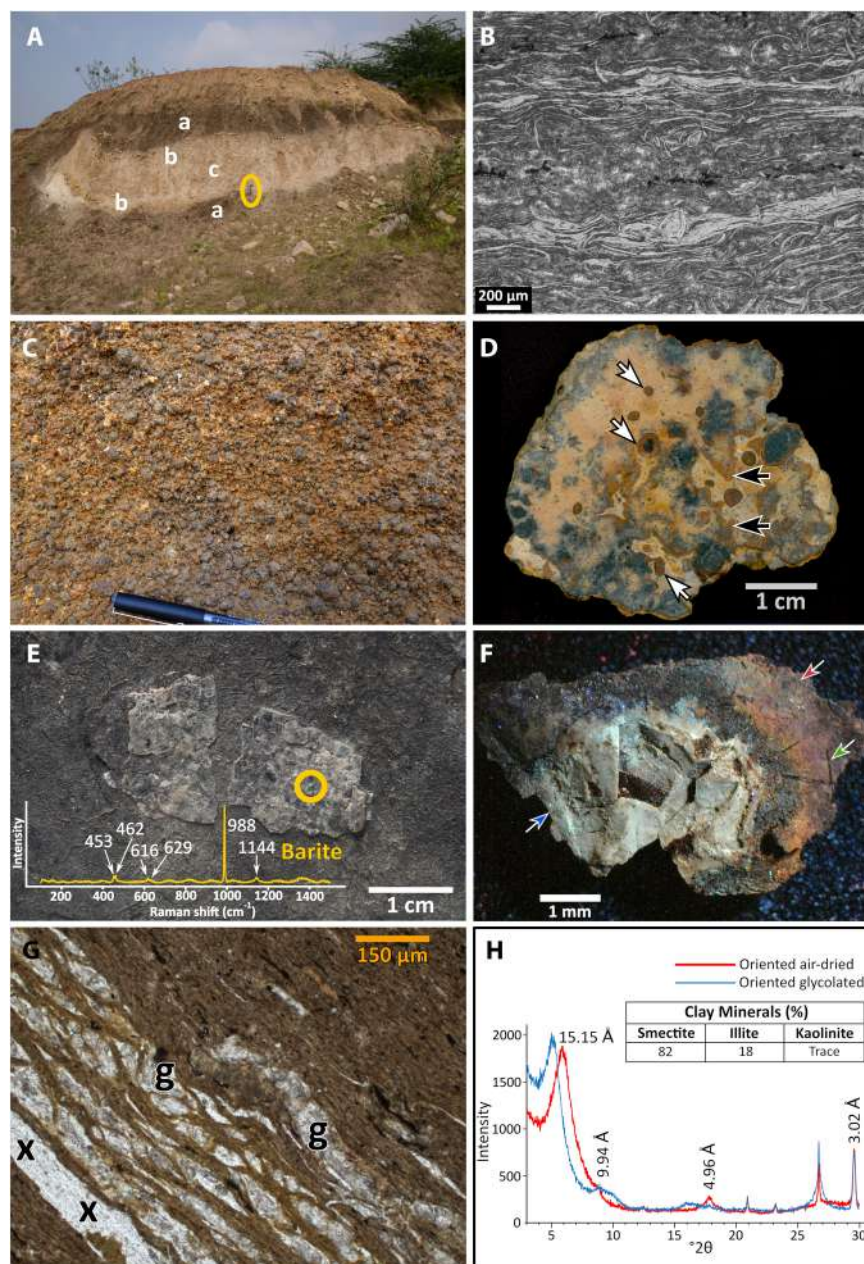


FIGURE 4 (A) Dark brown mudstones (a) enclosing lenticular body of yellowish-grey nodular limestone (b). Ferruginous coated grains occur in the middle part (c) of the nodular limestone body. Hammer (yellow oval) for scale. (B) Photomicrograph (under plane polarised light) showing bio-clastic laminites that occur above and below the ferruginous coated grain-rich part of the limestone. (C) Close-up view of the ferruginous-rich part of the limestone. Note poor sorting and roughness of the surface. Pen cap is 6 cm in length. (D) Polished section of the limestone showing floating ferruginous coated grains (white arrow) and iron oxide-lined contorted (dissolution?) surfaces (black arrow). (E) Bedding surface view of the laminated black ferruginous mudstone. Note, the abundance of carbonaceous plant fragments and baryte crystals. Raman spectrum for the crystal (o) showing the characteristic peaks of baryte. (F) A baryte nodule (blue arrow) in ferruginous mudstone showing characteristic light-yellow fluorescence under longwave ultraviolet (432 nm) illumination. Note the presence of carbonaceous plant matter (green arrow) in the ferruginous mudstone (red arrow). (G) Photomicrograph showing the lamination details in ferruginous mudstone (under plane polarised light) containing lamina-parallel-oriented plant debris (dark brown filaments). The lenses of gypsum nodules (g) disrupt the lamination in the centre of the photograph. Slide preparation defects are marked with x. (H) X-ray diffractogram of the <2µm fraction of the black ferruginous mudstone, showing the abundance of smectite (oriented air-dried diffractogram shows the main peak for smectite at 15.15 Å).

and goethite content (approx. 10:90; Figure 4E,G). Despite being less than 20µm thick, at the microscopic scale, they are wavy and discontinuous. Lamina surfaces are

strewn with carbonaceous plant fragments (Figure 4E). Baryte primarily occurs as nodules (5–6 mm in diameter) and very thin discontinuous lenses (millimetre-scale in

thickness) in between adjacent laminae of the ferruginous mudstones (Figure 4E,F). The laminae are curved around the baryte nodules, producing an irregular, discontinuous, wavy surface to the mudstone. These baryte nodules show a characteristic yellow colour under long wave ultraviolet illumination (Figure 4F). Gypsum occurs as discontinuous lenses (8–70 μm thick) limited in lateral extent (50–200 μm) between the iron oxide-rich laminae (Figure 4G). Mudstone laminae are found wrapped around the lenses. The XRD analysis of the clay fraction (<2 μm) shows an abundance of smectite with subordinate amounts of illite (Figure 4H).

4.2 | Microscopic features of the coated grains and associated sediments

In thin sections, a variety of ferruginous coated grains and detrital grains are found to be embedded in a groundmass of micritic-microsparitic calcite (Figure 5A). Within the groundmass, there are contorted surfaces that demarcate the boundary between various micritic regions (Figure 5A). Only one side of such surfaces are stained

due to the presence of yellow (in plane polarised light) iron oxides.

In general, the ferruginous coated grains contain a large and centrally located nucleus surrounded by a thick laminated cortex (0.1–1 mm thick). The nucleus is well differentiated from the cortex (Figure 5A). The nuclei of most coated grains are made up of very poorly sorted, angular, subhedral, silt to fine sand-sized detrital grains embedded in a groundmass of very dark, reddish brown (in places, dark greenish brown), amorphous iron oxides (Figure 5). The size of the detrital grains and the proportion of groundmass vary from grain to grain. The nucleus of some of the coated grains are made up almost entirely of iron oxides with a few dispersed silt-size detrital grains (Figure 5B,D). The detrital grains are mostly quartz; feldspars and micas are very rare. The quartz grains are monocrystalline and free of inclusions. In some places, they are fractured but are otherwise undeformed. Adjacent quartz grains do not show matching grain boundaries, and they do not become extinct simultaneously under cross polars with the rotation of the microscope stage.

For many grains, the outermost part of the cortex has been extensively replaced by spar calcite, which forms a corona around their periphery. Faint outlines of the

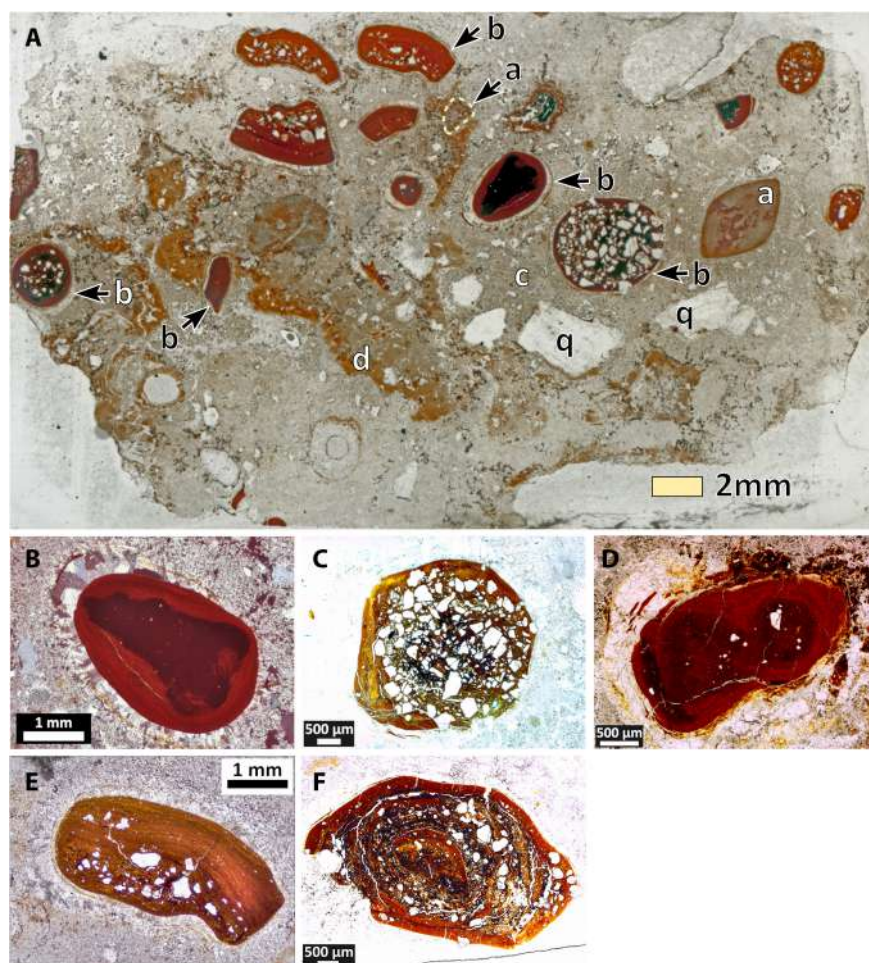


FIGURE 5 Photomicrographs showing the internal fabric of the ferruginous coated grains and the surrounding carbonate groundmass, in thin sections. (A) Panoramic view showing various types of coated and detrital grains embedded in a micrite-microspar. Chert fragments (a), ferruginous coated grains (b), micrite-microspar (c), dissolution surfaces lined by iron oxides (d) and quartz (q). Note the absence of bioclasts. Various types of coated grains: (B) Type 1, (C) Type 2, (D) Type 3, (E) Type 4 and (F) Type 5, all grains between crossed nicols. Note the sparry corona around the grains in B, D and E. The remnants of the replaced outermost part of the cortex are preserved in the spars.

pre-existing cortical lamination can be identified in these calcite crystals (Figure 5B,D,E). Some of the coated grains have lost their cortex altogether, and their nucleus is in direct contact with replacive calcite spars. The nucleus is generally rounded in shape. However, for some of the grains, it is conspicuously triangular in shape, having a gently incurved boundary (Figure 5B).

The cortical laminae are extremely thin (each about $<1\mu\text{m}$). They are arranged in groups that are 20 to $30\mu\text{m}$ thick (Figure 6A,B,D), representing laminasets (sensu. Campbell, 1967). Under plane polarised illumination, alternating dark reddish brown and lighter greenish/yellowish brown could be observed. Laminae are poorly defined, laterally discontinuous, as well as wavy and convoluted (Figure 6A,B,D). Under reflected light, they appear to consist of tangentially stacked, tiny flakes. Dispersed, fine-silt-sized, angular quartz grains and flaky clay minerals are present between the adjacent lamina (Figure 6E). The grains in the cortex are otherwise similar to the quartz grains in the nucleus, but, in most cases, they are significantly smaller in size. Most elongated quartz grains are oriented parallel to the lamination. However, some of the angular quartz grains are oriented orthogonally. Cortical laminae typically wrap around such grains and appear to have locally deformed due to the presence of the grain (Figure 6E).

The cortical laminae typically fill-up the depressions and irregularities present on the outer surface of the nucleus gradually (Figure 6B). Multiple generations of laminasets are present in most grains. Adjacent laminasets are slightly discordant with each other and separated by smooth, gently undulating surfaces. There is no concentration of clastic grains (quartz) along such surfaces. Some of the grains have been broken into pieces, and the individual fragments are enveloped by a later generation of cortical laminae. Based on the nature of the nucleus and cortical lamination, the ferruginous coated grains can be sub-divided into five types (see Table 2 for details):

Type 1 (Single—thickly multicoated): The grains have a single irregular-shaped nucleus and a cortex having comparable thickness. The nucleus contains silt-sized detrital (quartz) grains dispersed in iron oxide, while the cortex is iron oxide-rich, well laminated and made up of multiple laminasets (Figure 5B). These grains are similar to the Type A (Simple) grains of Reolid et al. (2008).

Type 2 (Single—thinly coated): The grains have a single large, equant nucleus and a comparatively thinner cortex. The nucleus contains closely packed sand-sized detrital grains. The cortex is iron oxide-rich, irregularly laminated and usually constituted of a single laminaset (Figure 5C). These grains are like the Type A (Simple) ooids described by Reolid et al. (2008).

Type 3 (Compound—multicoated): The grains have multiple nuclei surrounded by iron oxide-rich multiple laminasets (Figure 5D). The nucleus is similar to Type 1 grains. These grains are similar to the Type A (Complex) grains of Reolid et al. (2008).

Type 4 (Fragment—thinly coated): The nucleus is made up of a fragment of either Type 1 or Type 2 grains. It is surrounded by a thin yet well-laminated, iron oxide-rich cortex (Figure 5E). These are similar to the Type A (Fragmented) grains of Reolid et al. (2008).

Type 5 (Single—compound coated): These grains have a rounded nucleus similar to Type 1 or 2 but are surrounded by a cortex characterised by an alternate coating of smaller (silt-sized) and larger (sand-sized) quartz grains present along with the iron oxide-rich lamina (Figure 5F). This type of grain does not correspond to any of the types described by Reolid et al. (2008). However, deformed coated grains, similar to spastoliths (sensu. Guerrak, 1987; Reolid et al., 2008), were not observed.

4.3 | Sub-microscopic features and elemental compositions

The morphological distinctions between the cortex and nucleus, as well as between adjacent cortical laminasets, are not easily seen in the secondary electron images when viewed under SEM. In BSE images, however, the nucleus appears much brighter compared to the cortex (Figure 6B). The contact between the nucleus and cortex is very sharp. The groundmass inside the nucleus is predominantly made up of iron oxide(s), and it is uniform in terms of elemental composition, that is no compositional zoning has been observed (Figure 6C). The embedded detrital grains are angular in shape, and they appear dark in the BSE image. Their elemental composition is similar to that of quartz and Al-bearing silicates. The grain boundaries are sharp, and do not show any evidence of compositional gradation with the surrounding ferruginous groundmass.

In the cortex, lamination is clearly visible as ultrathin light and dark-coloured compositional bands, speckled with dark detrital grains (Figure 6B,D). The cortical laminae are typically discontinuous, wavy and convoluted in character (Figure 6D). Compared to the nucleus, the detrital grains are fewer and smaller in the cortical region. Elemental compositions suggest that, apart from quartz, a lesser amount of flake-like grains having elemental similarity with organic matter and mica are also present in the cortex. However, as in the nucleus, there is no compositional gradation between a detrital grain and its surrounding iron oxide(s).

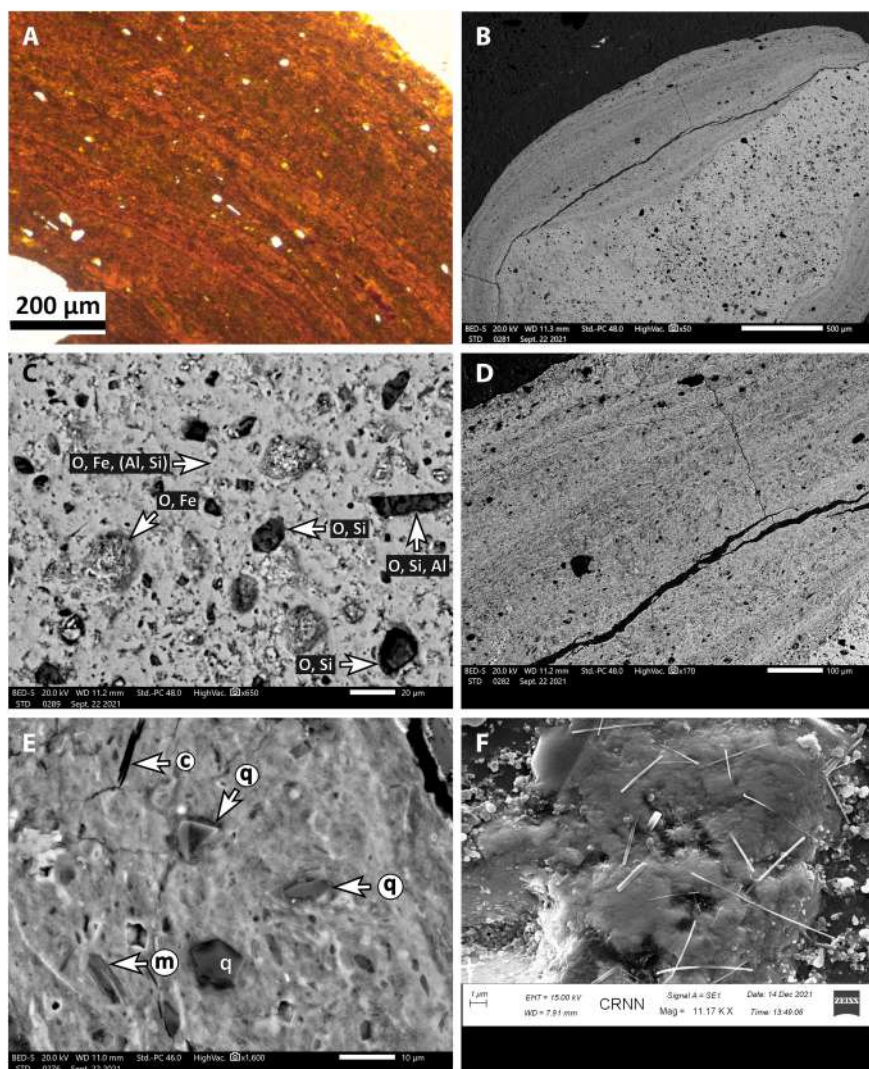


FIGURE 6 Microscopic and sub-microscopic features of the ferruginous coated grains. (A) Details of cortical lamina between parallel polars. Non-isopachous, slightly wavy nature of laminae, distinguished by colour tone and probably crystal size. Simple laminae are grouped into laminasets. Presence of truncation surface between adjacent laminasets. The presence of silt-size quartz grains where the elongated ones are oriented parallel to the lamination. (B) BSE image showing a lighter-coloured nucleus surrounded by comparatively less bright, layered cortex. The black regions in the upper left and lower right corners are made up of sparry calcite. Tiny detrital quartz grains present in the nucleus as well as those in the cortex are dark in colour. Scale bar 500 µm. (C) Close-up view of the nucleus. Note the amorphous character and elemental homogeneity of the iron-bearing groundmass. Also, note the very poor sorting and the angular shape of the quartz grains as well as their sharp boundary with the groundmass. The sub-rounded pits are possibly sample preparation defects. Scale bar 20 µm; Al, aluminium; Fe, iron; O, oxygen; Si, silicon. (D) BSE image showing the fine lamination in the cortex. Laminaset consisting of very thin crenulated simple laminae that alternate with thicker simple laminae. Scale bar 100 µm. (E) Detrital grains in the cortical lamination (upper left to lower right). The larger equant grains (q) and the smaller platy grains oriented parallel to the lamina are quartz. Cortical lamina has been deformed around a tangentially oriented platy quartz grain. The flake-like objects are possibly mica (m) and clay minerals (c). Scale bar 10 µm. (F) Enlarged view of the surface of the ferruginous coating showing a felt-like fabric made up of admixed acicular and fibrous crystals of iron oxides. Scale 1 µm.

At higher magnification, the surface of the coating appears as a mass of nearly amorphous iron oxide(s). In some places, however, clusters of tiny acicular crystals and filaments of iron oxide are found to be embedded in the mass of amorphous iron oxide(s) (Figure 6F). These crystals have faceted terminations. Their shapes resemble

goethite crystals synthesised in alkaline conditions (cf. Schwertmann & Taylor, 1989).

In general, the dominant elements in the nucleus of the coated grains, in decreasing order of abundance, are oxygen (49.9–60.0 wt%), iron (1.3–45.9 wt%), silicon (1.8–35.9 wt%) and aluminium (2.7–4.2 wt%). The

TABLE 2 Characteristics of the various types of ferruginous coated grains, Lower Jurassic Kota Limestone.

Grain types	Grain shape, Size (mm) and Nucleus: Cortex Ratio	Nucleus	Cortex	Thickness of cortex (mm)	Interpretation
Type 1: Single—Thickly Multicoated (Figure 5B)	Ellipsoidal; 2.8–4.1 1.8:1–4.5:1 ^a ; 1.1:1–2.1:1 ^b	<ul style="list-style-type: none"> Irregular outline Dark iron oxide rich Few angular silt-sized quartz 	<ul style="list-style-type: none"> Laminae wavy (distinguished by colour and crystal size) Lamina grouped into laminasets Outer laminaset smooth out depressions on older sets A few sub-rounded to sub-angular silt-sized quartz 	0.44–0.87 ^c ; 0.21–0.69 ^d	Fragment of ferruginous siltstone (ferricrete) coated multiple times in detritus-deficient environment
Type 2: Single—thinly coated (Figure 5C)	Spheroidal; 2.2–5.2 1.9:1–27.3:1 ^a ; 0.9:1–7:1 ^b	<ul style="list-style-type: none"> Rounded outline Detrital grain dominated (poorly sorted, angular fine/medium sand-sized quartz) 	<ul style="list-style-type: none"> Wavy irregular laminae Contain angular silt-sized quartz 	0.16–1.49 ^c ; 0.4–0.86 ^d	Formation of incipient coating around fragment of ferruginous sandstone (ferricrete) in detritus-deficient environment
Type 3: Compound—multicoated (Figure 5D)	Ellipsoidal; 3.8–4.1 2.1:1–2.3:1 ^a ; 0.9:1–1:1 ^b	<ul style="list-style-type: none"> Multiple Ferruginous coated grains of Type 1 Iron oxide rich Few angular sand-sized quartz 	<ul style="list-style-type: none"> Multiple laminasets Devoid of detrital grains 	0.76–0.98 ^c ; 0.98–1.13 ^d	Agglomerate of older ferruginous coated grains, like Type 1, coated multiple times in detritus-deficient environment
Type 4: Fragment—thinly coated (Figure 5E)	Bean-shaped to elongated; 1.7–5.0 10.8:1–35.3:1 ^a ; 2.3:1–10.1:1 ^b	<ul style="list-style-type: none"> Angular Fragments of ferruginous coated grain of Type 1 or Type 2 	<ul style="list-style-type: none"> Slightly wavy laminae Devoid of detrital grains 	0.12–0.2 ^c ; 0.25–0.63 ^d	Fragmentation of older ferruginous coated grain like Type 1 or 2, and formation of incipient coating in detritus-deficient environment
Type 5: Single—compound coated (Figure 5F)	Irregular ellipsoid; 7.0–7.5 0.3:1–0.4:1a; 0.2:1–0.3:1 ^b	<ul style="list-style-type: none"> Rounded Iron oxide rich Fragments of ferruginous coated grain of Type 1 or 2 	<ul style="list-style-type: none"> Multiple coats Alternation of silt to medium/fine sand-sized sub-rounded quartz-rich and iron oxide-rich lamina 	3.2–4.82 ^c ; 0.4–0.74 ^d	Fragment of older ferruginous grain (Type 1 or 2) coated multiple time in an environment receiving coarse detritus input

^aPreserved cortex.^bIncluding replaced cortex.^cPreserved.^dReplaced by calcite.

detrital grains in the cortex are made up of oxygen (27.1–69.2 wt%), silicon (1.3–69.2 wt%), iron (3.6–37.4 wt%), aluminium (0–11.4 wt%), potassium (0–10.4 wt%), magnesium (0–1.4 wt%) and sodium (0–1.1 wt%), and the lamina in the cortex are composed of oxygen (52.6–60.6 wt%), iron (21.2–36.3 wt%), aluminium (4.0–12.3 wt%) and silicon (2.0–12.2 wt%), both in decreasing order of abundance. The EDAX data indicates the presence of iron and sulphur throughout the grains, that is in both cortex and nucleus (Figure 7A,B,D). In contrast, although calcium occurs in abundance in the calcite cement outside the grains and in the cracks, it is almost completely absent inside the grains (Figure 7C). Cortices are enriched in aluminium compared to the nucleus (Figure 7E). Cortical lamination is defined by variations in aluminium and silicon content. Concentrations of sulphur and carbon are found to be uniform throughout these grains (3 and 4%, respectively) and at significantly lower concentrations than iron (23%). Features resembling pyrite crystals, however, were not detected in the BSE images.

4.4 | Mineralogical compositions

4.4.1 | XRD patterns

The X-ray diffractograms obtained from ferruginous coated grains manually separated from the host limestone are dominated by the large peaks of calcite in the residual cement and the quartz peak arising from the detrital grains (Figure 8A). Moreover, the peaks of goethite and haematite are ubiquitous in the diffractograms, together with small peaks suggestive of ferrihydrite in some of the samples (Figure 8A).

The presence of goethite has been identified based on the characteristic $d(110)$ and $d(111)$ peaks around 22.3° and $38.1^\circ 2\theta$. These peaks are slightly broadened. Average full width at half maximum (FWHM) is $0.3^\circ 2\theta$. The position of the $d(111)$ peak and the small width of the $d(111)$ and $d(110)$ peaks suggest minimal Al substitution in these goethites (about 2 mole%), according to the relationships proposed by Fitzpatrick and Schwertmann (1982) and Schulze (1984). Although the

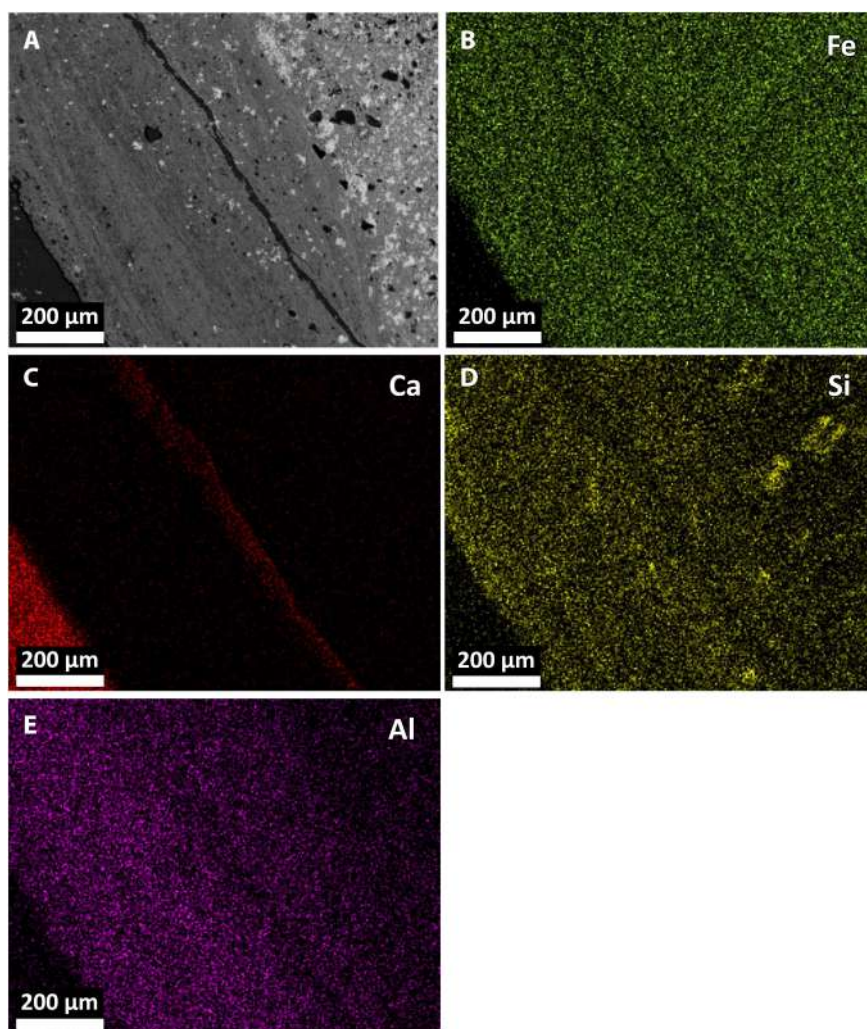


FIGURE 7 EDS analysis showing spatial distribution of major elements present in the ferruginous coated grains. (A) BSE image showing parts of nucleus (right) and cortex (middle). The dark area to the left represents calcite cement. (B–E) Elemental maps of the same field of view for iron (Fe), calcium (Ca), silicon (Si) and aluminium (Al), respectively. Note the near complete absence of calcium inside the grain and its abundance outside of it.

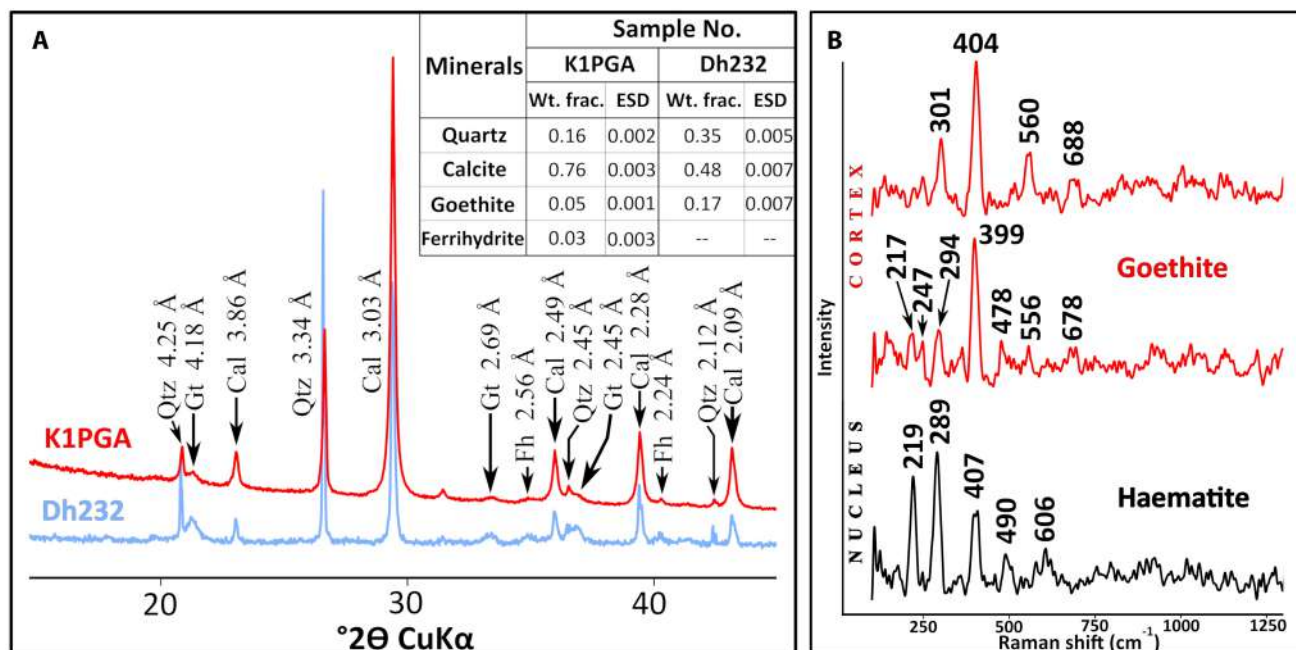


FIGURE 8 (A) Powder X-ray diffractograms of the ferruginous grains showing the presence of goethite (Gt). Large peaks of quartz (Qtz) and calcite (Cal) are present in all diffractograms due to the presence of quartz grains in the nucleus and cortex and the presence of calcite cement. Small peaks suggestive of the presence of ferrihydrite (Fh) are also present. (B) Laser Raman spectrum showing the presence of goethite in the cortex and the presence of haematite in the nucleus.

characteristic peaks of ferrihydrites (35° 2θ) could be detected, the computed quantity of the phase has been found to be very small (0.03 weight fraction; see inset in Figure 8A).

4.4.2 | Raman spectra

The Raman spectra obtained for the points lying in the cortical region of the coated grains display broad peaks (Figure 8B). The strongest one is located between 399 and 404 cm^{-1} , and the subsidiary peaks are located between 294 and 301 cm^{-1} . These peaks match fairly well with those of goethite (cf. RRuff ID: R050142) and the peaks reported by Hanesch (2009). The slight shift of the main peak (400 cm^{-1} peak) towards higher wavenumbers may indicate imperfect transformation of precursor iron hydroxide (like ferrihydrite) to goethite. However, the shift to a higher wavenumber is a characteristic signature of aluminium-substituted goethite (Liu et al., 2013). The goethite peaks in these samples suggest about 0–7% aluminium substitution based on the established relationships for the 400 and 300 cm^{-1} peaks suggested by Liu et al. (2013).

In contrast, the spectra for the amorphous iron oxide occurring in the nucleus of the grains show peaks similar

to haematite due to the presence of the peaks at 289 , 219 and 407 cm^{-1} (main), as well as those at 490 and 606 cm^{-1} (subordinate). These peaks correspond to those reported by Chukanov and Vigasina (2020) and match well with those of RRuff ID: R050300 (<https://rruff.info/>).

5 | DISCUSSION

5.1 | Salient features of the ferruginous grains and associated sediments

- The grains are found associated with freshwater lacustrine–palustrine limestones and ferruginous mudstones.
- Ferruginous mudstones contain evaporite minerals (gypsum and baryte), the clay mineral smectite and plant debris.
- Internally, the grains are devoid of carbonates, in spite of the fact that they are found embedded in limestones.
- The outermost iron oxide coating is replaced by calcite and not the other way round.
- A considerable number of detrital grains are present both in the nucleus and in the cortex.
- The main iron oxide phase is goethite. Haematite is the subordinate phase present in the nucleus.
- Aluminium substitution in the goethite is low.

5.2 | Has the cortex been formed in a stationary (diagenetic/paedogenetic) or in a non-stationary condition?

The similarity between the cortical laminae of carbonate and ferruginous coated grains, as well as the observed ferruginisation of the calcareous ooids and other calcareous coated grains, could suggest that the ferruginous grains are carbonate-coated grains that were extensively replaced by iron oxides during diagenesis (cf. Kimberley, 1974, 1979, 1980; Sorby, 1856). In this case, however, the complete absence of the cations of carbonates, for example calcium and magnesium (Table 3), in the nuclei and cortices of the ferruginous grains negates this mode of formation.

Furthermore, calcareous grain coatings generally form in environments that are starved of siliciclastic input (Tucker & Wright, 1990), and, as a consequence, the cortex of calcareous ooids and other calcareous coated grains are virtually free from detrital grains. In contrast, a large number of clastic grains occur in the cortices of these

ferruginous grains. Therefore, the ferruginous grains described here are probably primary coated grains made up of iron oxides.

On the other hand, extensive chemical weathering of exposed rock surfaces, especially under hot and humid conditions, can lead to the formation of residual soils rich in oxides of iron and aluminium. Laterite, bauxite and plinthite are some of the common varieties. Such soils are characterised by the development of boxwork structures with laminated walls. These laminae are formed due to the repeated formation of curved fractures and the development of hypocoatings on fracture walls. See Stoops and Marcelino (2018) for a model for the development of such laminae. Where they are very well developed, such laminae can assume a concentric appearance and may resemble a layered cortex. However, the main difference between a ferruginous grain coating and a lateritic boxwork lies in the fact that the latter is produced due to an advancing hypocoating front starting from the exposed surface of the soil cracks. Cracks of multiple orders are found to

TABLE 3 Elemental compositions of the ferruginous coated grains, Lower Jurassic Kota Limestone. The composition of the cement between the grains is also shown.

Region		Elements (wt%)										Total
		O	Na	Mg	Al	Si	K	Ca	Mn	Fe	Ba	
Cortex	Laminae	55.18	—	—	5.94	2.78	—	—	—	36.10	—	100
	Laminae	57.52	—	—	5.49	4.17	—	—	—	32.81	—	100
	Laminae	52.60	—	—	11.05	8.38	—	—	—	27.97	—	100
	Laminae	54.31	—	—	12.26	12.18	—	—	—	21.25	—	100
	Laminae	55.02	—	—	6.22	2.48	—	—	—	36.28	—	100
	Laminae	56.45	—	—	5.64	3.97	—	—	—	33.94	—	100
	Laminae	60.63	—	—	3.96	1.99	—	—	—	33.42	—	100
	Detrital grain	58.57	—	—	2.73	1.32	—	—	—	37.39	—	100
	Detrital grain	59.46	1.13	—	8.40	22.43	8.58	—	—	—	—	100
	Detrital grain	57.64	—	—	—	42.36	—	—	—	—	—	100
	Detrital grain	57.67	—	1.38	11.37	14.23	5.65	—	—	9.70	—	100
	Detrital grain	27.12	—	—	—	69.23	—	—	—	3.65	—	100
	Detrital grain	69.21	—	—	1.37	21.77	—	—	—	7.64	—	100
	Detrital grain	64.05	—	—	1.23	23.27	—	—	—	11.46	—	100
	Detrital grain	54.00	0.93	—	9.00	25.63	10.44	—	—	—	—	100
	Detrital grain	64.01	—	—	10.11	9.32	—	—	—	16.56	—	100
	Detrital grain	69.19	—	—	1.49	21.56	—	—	—	7.76	—	100
Diagenetic cement		64.04	—	—	—	—	—	35.96	—	—	—	100
		51.84	—	0.48	3.08	2.98	—	1.16	12.05	24.40	4.02	100
		47.82	—	—	2.61	3.52	—	1.58	31.49	2.43	10.56	100
Nucleus	Detrital grain	60.04	—	—	2.75	35.90	—	—	—	1.32	—	100
	Detrital grain	53.17	—	—	3.10	1.83	—	—	—	41.90	—	100
	Detrital grain	49.92	—	—	4.18	—	—	—	—	45.90	—	100
	Detrital grain	59.00	—	—	—	35.31	—	—	—	5.68	—	100

invade the core ('nucleus') from its perimeter. The core is made up of authigenic clays (commonly kaolinite) produced due to extensive weathering of the minerals in the pre-existing rocks. In contrast, ferruginous coated grains reported here have nuclei ('cores') that are dominated by iron oxides (haematite), without an appreciable clay mineral content.

Furthermore, Fitzpatrick and Schwertmann (1982) have demonstrated that a significant amount of aluminium is substituted in the goethite formed in paedogenic environments based on the results of an extensive study of the ferruginous soils. The very low aluminium substitution in goethite observed in the XRD analysis and Raman spectroscopy indicates a non-paedogenic origin of the goethite found in these grains.

Therefore, the observed coatings are unlikely to have been produced due to in situ alteration or replacement of an existing grain or ped. Rather, the cortex appears to have formed due to repeated precipitation of iron oxide on the surface of a non-stationary substrate.

5.3 | What is the source of iron and how does it reach the site of precipitation?

In a continent-interior setting, the iron reaching the basin can be produced mainly in three ways, for example weathering of aluminosilicates, oxidation of sulphides and geothermal enrichment (Kimberley, 1994; Kiyokawa et al., 2021; Preston et al., 2011; Stoops & Marcelino, 2018; Verplanck et al., 2007).

Under a hot and humid sub-tropical climate with pronounced seasonality of rainfall, laterites can form on the exposed surface of any type of parent rock. Chemical weathering of aluminosilicates involves dissolution of the mineral lattice and hydrolysis by acidic water during the rainy season. The soluble salts forming from these ions are washed away, leaving behind insoluble oxides and sulphates of iron, aluminium and silica (Bárdossy, 1982; Stoops & Marcelino, 2018). The initial product of such weathering is essentially kaolinised rock (saprolites). Therefore, erosion of laterite in the headwaters can provide iron oxide-rich particles and kaolinitic clays. The absence of kaolinite in the black ferruginous mudstone and the presence of smectite in profusion appear to rule out this mechanism. Further, Fitzpatrick and Schwertmann (1982), using a large number of samples from ferruginous soils, have demonstrated that during paedogenesis, a significant amount of aluminium is substituted in the goethite lattice. Both the XRD and Raman spectroscopy results for these samples indicate minimal Al substitution.

Alternatively, some modern river water contains high amounts of iron and other metals, due to the oxidation

of metallogenic sulphide deposits in the hinterland. The Rio Tinto River (Andalucía, Spain) and Animas River (Colorado, USA) are two such examples (see Church et al., 2007; Preston et al., 2011; Verplanck et al., 2007). Such sulphide deposits commonly contain quartz, iron oxide, baryte etc. as gangue minerals (Shanks et al., 2012). So, oxidation and erosion of sulphide deposits could have supplied detrital quartz and baryte, along with the iron oxides, to the depositional site. However, in this case, the barytes do not occur as detrital particles. They occur as authigenic nodules in the ferruginous mudstones. Baryte is chemically and mineralogically stable under surface conditions (cf. Bottrell & Newton, 2006), so the absence of detrital baryte negates the possibility of deriving the iron by oxidation of metallogenic sulphide deposits in the hinterland.

Another potential source of iron is from hydrothermal waters. Such waters can be enriched in dissolved ions of iron, sulphur and barium (Di Bella et al., 2019; Jones & Renaut, 2007; Kanellopoulos et al., 2019; Kimberley, 1994; Pirajno, 2020). Volcanogenic and geothermal enrichment in shallow marine and spring water has been documented by a large number of authors (Di Bella et al., 2019, 2021; Dreesen, 1989; Kimberley, 1994; Kiyokawa et al., 2021; Tazaki et al., 2006). Also, Chafetz et al. (1998) found that manganese-rich and iron-rich travertine shrubs are related to hot-water springs and interpreted them as being the result of bacterially induced precipitation.

Apart from these, in a foreland basin, Arenas et al. (2000) explained that the high iron, manganese and barium contents in Miocene fluvial tufa are suggestive of an additional supply of mineralised water related to springs. In that example, those elements were sourced by aquifers in Palaeozoic rocks of the Iberian Ranges. Additionally, rhyolitic tuff is known to decompose rapidly under sub-aerial conditions and is known to produce a large amount of iron (Klaes et al., 2023; Zúñiga et al., 2019).

For the Kota Formation a hydrothermal enrichment is relevant because the depositional area was situated in a rift basin. The extensional tectonics required for the formation of a rift involves thinning of the crust and the development of a system of normal faults at the basin margin. This generates a suitable setting for meteoric water (precipitation) to access a geothermal source and become enriched in certain ions that are usually not common in an alluvial system, for example barium.

5.4 | Under what bio-geochemical conditions are the iron oxides precipitated?

Soluble ferrous iron is stable at extremely low pH or under anaerobic conditions. In aerobic conditions, at

near-neutral pH and ambient temperature, it is oxidised spontaneously to the ferric (Fe^{3+}) form and is hydrolysed abiotically to insoluble ferric hydroxide. Precipitation begins with the formation of ferrihydrite. It is a poorly crystalline and metastable form of iron oxyhydroxide that rapidly transforms to more thermodynamically stable iron (oxyhydr-) oxides like goethite ($\alpha\text{-FeOOH}$) and haematite ($\alpha\text{-Fe}_2\text{O}_3$) (cf. Chen et al., 2022; Cornell & Schwertmann, 2003). Iron-oxidising microbes, such as acidithiobacillus or microaerophiles that colonise the oxic-anoxic boundary, can mediate the precipitation. Although the nucleation of haematite and goethite from ferrihydrite can occur concurrently (Chen et al., 2022), the formation of goethite is favoured over haematite in acidic (around pH4) and in alkaline (around pH10) solutions (Schwertmann & Murad, 1983). Haematite is preferred near a neutral pH. Therefore, the dominance of goethite in the cortex may suggest precipitation in either acidic or alkaline waters. In contrast, the haematite in the nucleus suggests near-neutral pH (cf. Chen et al., 2022; Schwertmann & Murad, 1983).

Experimental studies have noted that, under ambient temperature, the form of goethite crystals depends on the pH of the solution (Cornell & Schwertmann, 2003; Schwertmann & Murad, 1983; Schwertmann & Taylor, 1989). The well-formed acicular goethite crystals noted in these samples (Figure 6F) resemble those forming in alkaline solutions. Again, the crystalline form of goethite also depends on the degree of aluminium substitution (cf. Cornell & Schwertmann, 2003). The shape of goethite crystals in the cortex resembles that of low aluminium-substituted goethites reported by Cornell and Schwertmann (2003) and corresponds to low aluminium substitution values found in the XRD and Raman studies.

5.5 | A model for the depositional setting

The stratigraphic position of the carbonate bodies, which contain ferruginous grains, and the black ferruginous mudstones indicates a depositional setting intermediate between a siliciclastic lake-margin environment and a carbonate-precipitating wetland system in a continental rift basin. The laminated ferruginous mudstones containing plant litter and the lenticular limestones containing freshwater bivalves indicate an overall depositional environment that is similar to a vegetated marsh or bog. This depositional setting is similar to the immediately overlying palustrine succession that has been interpreted as a carbonate-precipitating wetland by Goswami et al. (2018) and Goswami and Ghosh (2020). The difference being the dominance of ferruginous mudstones

and the paucity of limestones compared to the palustrine succession.

Due to the dominance of iron oxides and the presence of carbonaceous plant litters, these ferruginous mudstones bear resemblance to iron-bog deposits (cf. Church et al., 2007; Kaczorek & Sommer, 2003; Stanton et al., 2007; Verplanck et al., 2007). However, the water of iron bogs is known to be acidic, and their deposits commonly contain kaolinite in the clay phase and jarosite in the sulphate phase (Renaut & Jones, 2011; Des Marais & Walter, 2019; Pirajno, 2020). On the other hand, the precipitation of carbonates requires an alkaline medium. Furthermore, although certain members of the smectite group of clay minerals are known to form in thermal waters (Des Marais & Walter, 2019; Pirajno, 2020), they are not usually found associated with sulphate minerals, as in this case. Therefore, episodic influxes of Fe-rich spring water in a shallow vegetated alkaline pool may be envisaged (Figure 9).

The concentration of barium is very low in freshwater conditions (Griffith & Paytan, 2012; Hanor, 2000). The occurrence of baryte nodules in the mudstones additionally points towards an influx of hydrothermally barium-enriched water (see also Elswick & Maynard, 2014). In a continental rift environment, enrichment of spring water can take place by hydrothermal processes (cf. Renaut & Jones, 2011; Renaut & Owen, 2023; Chorowicz, 2005; Des Marais & Walter, 2019; Pirajno, 2020). In the present case, the basin-bounding faults might have provided conduits for meteoric water to reach iron-rich and barium-rich rocks lying at shallow sub-surface, and allowed the enriched waters to mix with surface water. In the absence of features like travertine or siliceous sinter, it is probably that the enriched water, when it reached the surface, was near ambient temperature.

Increased acidity induced by the episodic influx of waters enriched in iron and barium could have been neutralised due to mixing with alkaline surface waters. The thin sandy sheet-flood deposits (Figure 3C) that are preserved in the succession bear testimony to the events of enhanced freshwater influxes. The lenticular carbonate bodies containing the ferruginous coated grains admixed with detrital quartz grains possibly formed near the points of discharge of surface (meteoric) water. A return to more alkaline conditions would have allowed the resumption of precipitation of microbially mediated freshwater carbonates and the survival of the bivalves. A similar mechanism of pH changes has been suggested by Jones and Renaut (2007) from acid hot springs in the Waiotapu geothermal area of North Island, New Zealand. In this case, the acidity of the water could have varied over time due to (a) input of iron and barium-enriched waters, (b) fluctuations in meteoric water discharge and (c) the progressive formation of iron oxides from solution.

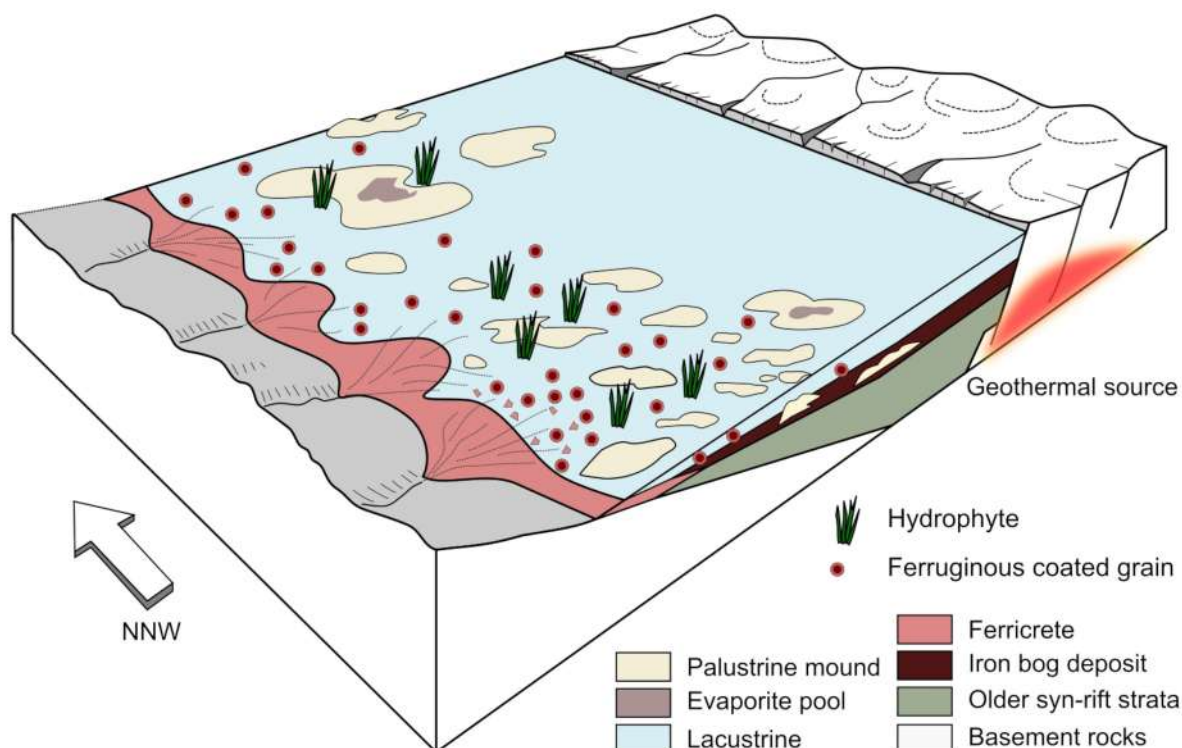


FIGURE 9 A schematic diagram depicting the sedimentary environments, associated processes and deposits in the continental rift basin during the formation of the ferruginous coated grains. The graben is about 30 km wide.

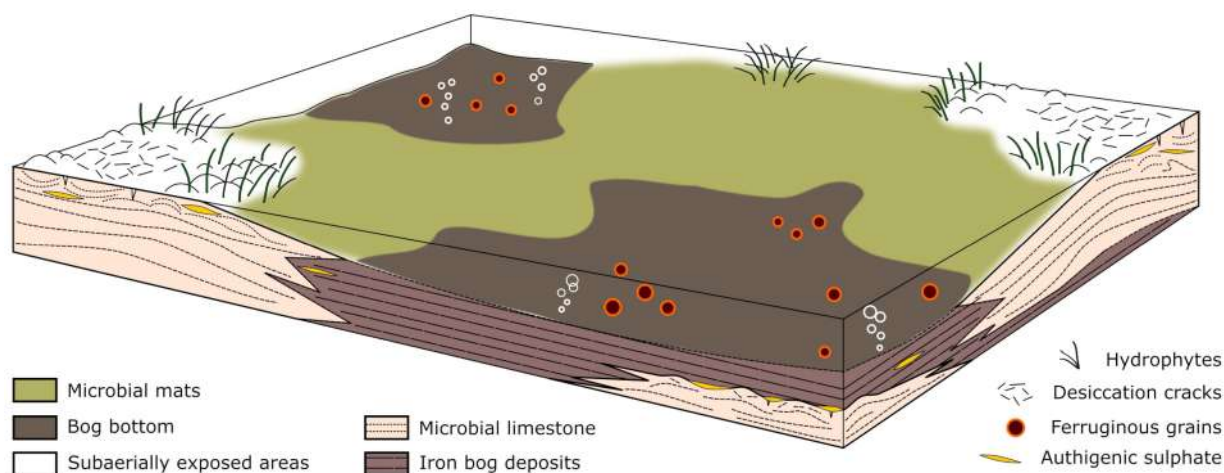


FIGURE 10 A schematic diagram showing the details of the site of formation of the ferruginous coated grains. The area depicted is about 10 km².

The phases of increased acidity might have produced the observed dissolution vugs in the carbonate bodies (Figure 4D), and the vug surfaces are subsequently coated by iron oxides. The observed dissolution of the outer cortex of the ferruginous coated grains, the cementation of the grains by sparry calcite and the formation of newer generations of cortex all might be related to changes in water level, pH of the water and discharge of the inlet streams.

The oxygenated waters of the shallow vegetated pool are probably to have provided a conducive environment for widespread precipitation of iron oxides through mediation by iron-oxidising microbes in a near-neutral pH. These precipitates quickly cemented the terrigenous clastics arriving at the shore from the hinterland and formed ferricretes along the margin. During the phases of higher freshwater discharge, these ferricretes were eroded, and their fragments were transported to comparatively deeper

waters. At those sites, ferruginous coating formed around the loose ferricrete fragments (Figure 10).

6 | CONCLUSIONS

The internal fabric of the studied Lower Jurassic ferruginous coated grains shows that an accretionary cortex has formed around loose fragment(s) of ferricretes. These ferruginous coatings are primary in nature and do not represent replaced calcareous coated grains. Despite certain mineralogical and textural similarities with laterites/ferruginous pisolites in plinthites, the layered cortex, in this case, did not form as an in situ weathering product of iron-bearing material. Apart from the ferricrete fragments, ferruginous coatings have also developed around other type of substrates available at the site of precipitation.

In the literature, ferruginous coated grains have been mainly reported from various (shallow) marine environments, where the formation of grain coatings has been explained by invoking a mechanism similar to that of calcareous coated grains. The weathering of land surfaces and marine volcanism might have provided the iron.

In comparison, ferruginous grains having concentric lamination and occurring in continental deposits have been mostly considered as a product of soil-forming processes. This study demonstrates that ferruginous coatings can form in a shallow freshwater lake-margin environment under certain conditions. The first and foremost requirement is a copious supply of dissolved iron. In this particular case, that condition was possibly accomplished due to hydrothermal enrichment of the spring water feeding an iron bog. The second requirement is a conducive bio-geochemical environment for the precipitation of iron hydroxides. That was attained by the presence of oxygenated waters in a freshwater wetland and the thriving iron-oxidising microbes in it.

ACKNOWLEDGEMENTS

The authors acknowledge the financial and infrastructural facilities provided by the Indian Statistical Institute, India, for conducting this research. Authors remain thankful to Mr. Pratyush Sengupta of the Centre of Nano-Sciences, University of Calcutta, Kolkata, India and to Dr. Manas Ghosh of Indian Association of Cultivation of Sciences, Kolkata, India, for their expert help in scanning electron microscopy and Raman spectroscopy, respectively. The authors also thank Mr. Mithun Naskar for his help in field data collection. The authors remain thankful to the reviewers and editors for providing insightful comments and constructive suggestions, which helped to improve the manuscript.

DATA AVAILABILITY STATEMENT

The data that support the findings of this study are available from the corresponding author upon reasonable request.


ORCID

Shantanu Datta  <https://orcid.org/0009-0008-7936-7257>

Arnab Sain  <https://orcid.org/0000-0001-6266-8784>

Suparna Goswami  <https://orcid.org/0000-0001-9240-8780>

Parthasarathi Ghosh  <https://orcid.org/0000-0002-5658-3802>

Concepción Arenas Abad  <https://orcid.org/0000-0002-4212-0524>

REFERENCES

- Acharyya, S.K. (2000) Tectonic setting and nature of the Gondwanic Indian crust. In Proceedings volume, International Seminar, Precambrian crust in eastern and central India. *Geological Survey of India Special Publication*, 57, 1–8.
- Anand, R.R. & Paine, M. (2002) Regolith geology of the Yilgarn Craton, Western Australia: implications for exploration. *Australian Journal of Earth Sciences*, 49(1), 3–162. <https://doi.org/10.1046/j.1440-0952.2002.00912.x>
- Anand, R.R. & Verrall, M. (2011) Biological origin of minerals in pisolites in the Darling Range of Western Australia. *Australian Journal of Earth Sciences*, 58(7), 823–833. <https://doi.org/10.1080/08120099.2011.597562>
- Arenas, C., Gutiérrez, O.C. & Sancho, C. (2000) Sedimentology and geochemistry of fluvio-lacustrine tufa deposits controlled by evaporite solution subsidence in the central Ebro Depression, NE Spain. *Sedimentology*, 47(4), 883–909. <https://doi.org/10.1046/j.1365-3091.2000.00329.x>
- Aurell, M., Fernandez-Lopez, S. & Melendez, G. (1994) The Middle–Upper Jurassic oolitic ironstone level in the Iberian range (Spain). Eustatic implications. *Geobios*, 27, 549–561. [https://doi.org/10.1016/S0016-6995\(94\)80220-3](https://doi.org/10.1016/S0016-6995(94)80220-3)
- Bandyopadhyay, S. (2011) Non-marine Triassic Vertebrates of India. In: Calvo, L.O., Porfiri, J.O., Gonzalez, J. & Santos, D.D. (Eds.) *Paleontología y Dinosaurios desde América Latina EDIUNC*. Mendoza, Argentina: Editorial de la Universidad Nacional de Cuyo, pp. 33–46.
- Bandyopadhyay, S., Gillette, D.D., Ray, S. & Sengupta, D.P. (2010) Osteology of *Barapasaurus tagorei* (Dinosauria: Sauropoda) from the early Jurassic of India. *Palaeontology*, 53(3), 533–569. <https://doi.org/10.1111/j.1475-4983.2010.00933.x>
- Bandyopadhyay, S. & Rudra, D.K. (1985) Upper Gondwana stratigraphy, north of the Pranhita-Godavari confluence, Southern India. *Geological Society of India*, 26(4), 261–266.
- Bandyopadhyay, S. & Sengupta, D.P. (2006) Vertebrate faunal turnover during the Triassic–Jurassic transition: an Indian scenario. *New Mexico Museum of Natural History & Science Bulletin*, 37, 77–85.
- Bárdossy, G. (1982) *Karst bauxites: bauxite deposits on carbonate rocks*. Budapest: Akadémiai Kiado.
- Bekker, A., Slack, J.F., Planavsky, N., Krapez, B., Hofmann, A., Konhauser, K.O. & Rouxel, O.J. (2010) Iron formation: the sedimentary product of a complex interplay among mantle,

- tectonic, oceanic, and biospheric processes. *Economic Geology*, 105(3), 467–508. <https://doi.org/10.2113/gsecongeo.105.3.467>
- Berendsen, P., Doveton, J.H. & Speczik, S. (1992) Distribution and characteristics of a Middle Ordovician oolitic ironstone in northeastern Kansas based on petrographic and petrophysical properties: a Laurasian ironstone case study. *Sedimentary Geology*, 76(3–4), 207–219. [https://doi.org/10.1016/0037-0738\(92\)90084-5](https://doi.org/10.1016/0037-0738(92)90084-5)
- Biswas, S.K. (1999) A review on the evolution of rift basins in India during Gondwana with special reference to western Indian basins and their hydrocarbon prospects. *Proceedings-Indian National Science Academy Part A*, 65(3), 261–284.
- Biswas, S.K. (2003) Regional tectonic framework of the Pranhita-Godavari basin, India. *Journal of Asian Earth Sciences*, 21(6), 543–551. [https://doi.org/10.1016/S1367-9120\(02\)00145-1](https://doi.org/10.1016/S1367-9120(02)00145-1)
- Bottrell, S.H. & Newton, R.J. (2006) Reconstruction of changes in global sulfur cycling from marine sulfate isotopes. *Earth-Science Reviews*, 75(1–4), 59–83. <https://doi.org/10.1016/j.earscirev.2005.10.004>
- Brett, C.E., McLaughlin, P.I., Histon, K., Schindler, E. & Ferretti, A. (2012) Time-specific aspects of facies: state of the art, examples, and possible causes. *Palaeogeography, Palaeoclimatology, Palaeoecology*, 367, 6–18. <https://doi.org/10.1016/j.palaeo.2012.10.009>
- Burkhalter, R.M. (1995) Ooidal ironstones and ferruginous microbialites: origin and relation to sequence stratigraphy (Aalenian and Bajocian, Swiss Jura mountains). *Sedimentology*, 42(1), 57–74. <https://doi.org/10.1111/j.1365-3091.1995.tb01271.x>
- Campbell, C.V. (1967) Lamina, laminaset, bed and bed-set. *Sedimentology*, 8(1), 7–26. <https://doi.org/10.1111/j.1365-3091.1967.tb01301.x>
- Casshyap, S.M. & Tewari, R.C. (1991) Depositional model and tectonic evolution of Gondwana basins. In: Venkatachala, B.S. & Maheswari, H.K. (Eds.) *Indian Gondwana*, Vol. 21. Bangalore: Memoirs of the Geological Survey of India, pp. 95–206.
- Chafetz, H.S., Akdim, B., Julia, R. & Reid, A. (1998) Mn- and Fe-rich black travertine shrubs; bacterially (and nanobacterially) induced precipitates. *Journal of Sedimentary Research*, 68(3), 404–412. <https://doi.org/10.2110/jsr.68.404>
- Chakraborty, C., Mandal, N. & Ghosh, S.K. (2003) Kinematics of the Gondwana basins of peninsular India. *Tectonophysics*, 377(3–4), 299–324. <https://doi.org/10.1016/j.tecto.2003.09.011>
- Chatterjee, G.C. & Ghosh, P.K. (1970) Tectonic framework of the Peninsular Gondwanas of India. *Records of Geological Survey of India*, 98(2), 1–15.
- Chatterjee, S. & Roy Chowdhuri, T.K. (1974) Triassic Gondwana vertebrates from India. *Indian Journal of Earth Sciences*, 1, 96–112.
- Chauvel, J.J. & Massa, D. (1981) Paléozoïque de Lybie occidentale. Constantes géologiques et pétrographiques. Signification des niveaux ferrugineux oolithiques. *Notes et Mémoires de la Compagnie Française des Pétroles*, 16, 25–66.
- Chen, S.A., Heaney, P.J., Post, J.E., Eng, P.J. & Stubbs, J.E. (2022) Hematite-goethite ratios at pH 2–13 and 25–170°C: a time-resolved synchrotron X-ray diffraction study. *Chemical Geology*, 606, 120995. <https://doi.org/10.1016/j.chemgeo.2022.120995>
- Chen, S., Zeng, M., Tian, J., Ren, K., Wang, B., Zhao, Z., Chen, X., Ethensohn, F.R. & Adatte, T. (2023) Microbe-mediated, marine authigenic formation of ooidal chamosite: insights from upper Ordovician carbonates of the South-Western Yangtze platform (China). *Sedimentology*, 70(5), 1655–1678. <https://doi.org/10.1111/sed.13091>
- Chorowicz, J. (2005) The east African rift system. *Journal of African Earth Sciences*, 43(1–3), 379–410. <https://doi.org/10.1016/j.jafrearsci.2005.07.019>
- Chukanov, N.V. & Vigasina, M.F. (2020) Raman Spectra of Minerals. In: *Vibrational (infrared and Raman) spectra of minerals and related compounds*. Springer mineralogy. Cham: Springer. https://doi.org/10.1007/978-3-030-26803-9_4
- Church, S.E., Owen, R.J., Von Guerard, P., Verplanck, P.L., Kimball, B.A. & Yager, D.B. (2007) The effects of acidic mine drainage from historical mines in the Animas River watershed, San Juan County, Colorado—What is being done and what can be done to improve water quality? In: DeGraff, J.V. (Ed.) *Understanding and Responding to Hazardous Substances at Mine Sites in the Western United States*. Boulder, CO: The Geological Society of America Reviews in Engineering Geology, XVII, 47–83. [https://doi.org/10.1130/2007.4017\(04\)](https://doi.org/10.1130/2007.4017(04))
- Collin, P.Y., Loreau, J.P. & Courville, P. (2005) Depositional environments and iron ooid formation in condensed sections (Callovian–Oxfordian, south-eastern Paris basin, France). *Sedimentology*, 52(5), 969–985. <https://doi.org/10.1111/j.1365-3091.2005.00728.x>
- Cornell, R.M. & Schwertmann, U. (2003) *The iron oxides: structure, properties, reactions, occurrences, and uses*. Weinheim: Wiley-vch. <https://doi.org/10.1002/3527602097>
- Dahanayake, K. & Krumbein, W.E. (1986) Microbial structures in oolitic iron formations. *Mineralium Deposita*, 21, 85–94. <https://doi.org/10.1007/BF00204266>
- Dasgupta, S., Banerjee, S. & Ghosh, P. (2022) Petrographical and Geochemical Study of Syn-Rift Sediments, Pranhita-Godavari Intracratonic Gondwana Basin, India: genesis and paleo-environmental implications. *Geosciences*, 12(6), 230. <https://doi.org/10.3390/geosciences12060230>
- Dasgupta, S., Ghosh, P. & Gierlowski-Kordesch, E.H. (2017) A discontinuous ephemeral stream transporting mud aggregates in a continental rift basin: the Late Triassic Maleri Formation, India. *Journal of Sedimentary Research*, 87(8), 838–865. <https://doi.org/10.2110/jsr.2017.47>
- Des Marais, D.J. & Walter, M.R. (2019) Terrestrial hot spring systems: introduction. *Astrobiology*, 19(12), 1419–1432. <https://doi.org/10.1089/ast.2018.1976>
- Deverin, L. (1945) Etude pétrographique des minerais de fer oolithiques du Dogger des Alpes suisses. *Beiträge zur Geologie der Schweiz. Geotechnische Serie*, 13(2), 115.
- Di Bella, M., Sabatino, G., Quartieri, S., Ferretti, A., Cavalazzi, B., Barbieri, R., Foucher, F., Messori, F. & Italiano, F. (2019) Modern iron ooids of hydrothermal origin as a proxy for ancient deposits. *Scientific Reports*, 9(1), 7107. <https://doi.org/10.1038/s41598-019-43181-y>
- Di Bella, M., Pirajno, F., Sabatino, G., Quartieri, S., Barbieri, R., Cavalazzi, B., Ferretti, A., Danovaro, R., Romeo, T., Andaloro, F. & Esposito, V. (2021) Rolling ironstones from earth and mars: terrestrial hydrothermal ooids as a potential analogue of martian spherules. *Minerals*, 11(5), 460. <https://doi.org/10.3390/min11050460>
- Doebelin, N. & Kleeberg, R. (2015) Profex: a graphical user interface for the Rietveld refinement program BGMN. *Journal of Applied Crystallography*, 48(5), 1573–1580. <https://doi.org/10.1107/S1600576715014685>
- Downs, R.T. (2006) The RRUFF Project: an integrated study of the chemistry, crystallography, Raman and infrared spectroscopy

- of minerals. In Program and Abstracts of the 19th General Meeting of the International Mineralogical Association in Kobe, Japan.
- Dreesen, R. (1989) Oolitic ironstones as event-stratigraphical marker beds within the Upper Devonian of the Ardenno-Rhenish Massif. In: Young, T.P. & Taylor, W.E.G. (Eds.) *Phanerozoic ironstones*. London: Geological Society, Special Publications, 46(1), 65–78. <https://doi.org/10.1144/GSL.SP.1989.046.01.08>
- Dubois, D. (1979) Etude géologique des formations oolitiques ferrugineuses du bassin des Jullemeden (République du Niger). PhD Thesis University, Niamey, Niger.
- Dubois, D. & Icole, M. (1977) Les formation à oolite ferrugineuses du Bassin des Jullemeden (Niger Occidental) et les cuirassement ultérieurs. Abstract 5th Ann Reunion, Sci. de la Terre, 207.
- Elswick, E.R. & Maynard, J.B. (2014) Bedded Barite deposits: environments of deposition, styles of mineralization, and tectonic settings. In: MacKenzie, F.T. (Ed.) *Treatise of geochemistry 2nd edition. 781 Volume 9, Sediments, Diagenesis, and Sedimentary Rocks*. Amsterdam: Elsevier, pp. 629–655. <https://doi.org/10.1016/B978-0-08-095975-7.00720-8>
- Fitzpatrick, R.W. & Schwertmann, U. (1982) Al-substituted goethite—an indicator of pedogenic and other weathering environments in South Africa. *Geoderma*, 27, 335–347. [https://doi.org/10.1016/0016-7061\(82\)90022-2](https://doi.org/10.1016/0016-7061(82)90022-2)
- Formozova, L.N. (1959) *Zheleznye rudy Severnogo Priaral'ya. Iron ores of the Northern Near-Aral region*. Moscow: Trudy Geologicheskogo Instituta Moskva, p. 20.
- Garcia-Frank, A., Ureta, S. & Mas, R. (2012) Iron-coated particles from condensed Aalenian–Bajocian deposits: evolutionary model (Iberian Basin, Spain). *Journal of Sedimentary Research*, 82(12), 953–968. <https://doi.org/10.2110/jsr.2012.75>
- Ghosh, P. & Sengupta, D.P. (2020) Geodynamics of Gondwanaland. In: Gupta, N. & Tandon, S. (Eds.) *Geodynamics of the Indian plate: evolutionary perspectives*. Springer geology. Cham: Springer, pp. 213–232. https://doi.org/10.1007/978-3-030-15989-4_7
- Goswami, S. (2021) Sedimentology of the Limestone Interval and its Underlying Siliciclastic Succession of the Kota Formation, Pranhita-Godavari Gondwana Basin, India. PhD thesis submitted to University of Calcutta <http://hdl.handle.net/10603/461058>
- Goswami, S. & Ghosh, P. (2020) Evolution of sedimentation pattern in a continental rift basin of India, between the Late Triassic and the early Middle Jurassic: tectonic and climatic controls. *Sedimentary Geology*, 405, 105679. <https://doi.org/10.1016/j.sedgeo.2020.105679>
- Goswami, S. & Ghosh, P. (2021) Freshwater Microbialites in Early Jurassic Fluvial Strata of the Pranhita-Godavari Gondwana Basin, India. In: Rosen, M.R., Finkelstein, D.B., Park Boush, L. & Pla-Pueyo, S. (Eds.) *Limnogeology: progress, challenges and opportunities: a tribute to Elizabeth Gierlowski-Kordesch, syntheses in limnogeology*. Cham: Springer, pp. 549–578. https://doi.org/10.1007/978-3-030-66576-0_18
- Goswami, S., Gierlowski-Kordesch, E. & Ghosh, P. (2018) Sedimentology of the Early Jurassic limestone beds of the Kota Formation: record of carbonate wetlands in a continental rift basin of India. *Journal of Paleolimnology*, 59, 21–38. <https://doi.org/10.1007/s10933-016-9918-y>
- Griffith, E.M. & Paytan, A. (2012) Barite in the ocean—occurrence, geochemistry and palaeoceanographic applications. *Sedimentology*, 59(6), 1817–1835. <https://doi.org/10.1111/j.1365-3091.2012.01327.x>
- Guerrak, S. (1987) Metallogenesis of cratonic oolitic ironstone deposits in the Bled el Mass, Azzel Matti, Ahnet and Mouydir basins, Central Sahara, Algeria. *Geologische Rundschau*, 76, 903–922. <https://doi.org/10.1007/BF01821072>
- Gygi, R.A. (1981) Oolitic iron formations: marine or not marine? *Eclogae Geologicae Helveticae*, 74, 233–254.
- Hanesch, M. (2009) Raman spectroscopy of iron oxides and (oxy) hydroxides at low laser power and possible applications in environmental magnetic studies. *Geophysical Journal International*, 177, 941–948. <https://doi.org/10.1111/j.1365-246X.2009.04122.x>
- Hanor, J.S. (2000) Barite–celestine geochemistry and environments of formation. *Reviews in Mineralogy and Geochemistry*, 40(1), 193–275. <https://doi.org/10.2138/rmg.2000.40.4>
- Heikoop, J.M., Tsujita, C.J., Risk, M.J., Tomascik, T. & Mah, A.J. (1996) Modern iron ooids from a shallow-marine volcanic setting: Mahengetang, Indonesia. *Geology*, 24(8), 759–762. [https://doi.org/10.1130/0091-7613\(1996\)024%3C0759:MIOFA S%3E2.3.CO;2](https://doi.org/10.1130/0091-7613(1996)024%3C0759:MIOFA S%3E2.3.CO;2)
- Heim, A. (1916) Monographie der Churfürsten-Matterhorn Gruppe. 3. Teil: lithogenesis. Beitr Geol Karte Schweiz NF, 20.
- Jain, S.L. (1980) The continental lower Jurassic fauna from the Kota formation, India. In: Jacob, L.L. (Ed.) *Aspects of vertebrate history*. Flagstaff: Museum of Northern Arizona Press, pp. 99–123.
- Jain, S.L., Robinson, P.L. & Chowdhury, T. (1964) A new vertebrate fauna from the Triassic of the Deccan, India. *Geological Society of London*, 120, 115–124. <https://doi.org/10.1144/gsjgs.120.1.0115>
- James, H.E. & Van Houten, F.B. (1979) Miocene goethitic and chamositic oolites, northeastern Colombia. *Sedimentology*, 26(1), 125–133. <https://doi.org/10.1111/j.1365-3091.1979.tb00342.x>
- Jones, B. & Renaut, R.W. (2007) Selective mineralization of microbes in Fe-rich precipitates (jarosite, hydrous ferric oxides) from acid hot springs in the Waiotapu geothermal area, North Island, New Zealand. *Sedimentary Geology*, 194, 77–98. <https://doi.org/10.1016/j.sedgeo.2006.05.025>
- Kaczorek, D. & Sommer, M. (2003) Micromorphology, chemistry, and mineralogy of bog iron ores from Poland. *Catena*, 54, 393–402. [https://doi.org/10.1016/S0341-8162\(03\)00133-4](https://doi.org/10.1016/S0341-8162(03)00133-4)
- Kanellopoulos, C., Thomas, C., Xirokostas, N. & Ariztegui, D. (2019) Banded iron travertines at the Ilia hot spring (Greece): an interplay of biotic and abiotic factors leading to a modern banded iron formation analogue? *The Depositional Record*, 5(1), 109–130. <https://doi.org/10.1002/dep.2.55>
- Kelley, V.C. (1951) Oolitic iron deposits of New Mexico. *AAPG Bulletin*, 35(10), 2199–2228. <https://doi.org/10.1306/3D934331-16B1-11D7-8645000102C1865D>
- Kholodov, V.N., Nedumov, R.I. & Golubovskaya, E.V. (2012) Facies types of sedimentary iron ore deposits and their geochemical features: communication 1. Facies groups of sedimentary ores, their lithology, and genesis. *Lithology and Mineral Resources*, 47, 447–472. <https://doi.org/10.1134/S0024490212060053>
- Kimberley, M.M. (1974) Origin of iron ore by diagenetic replacement of calcareous oolite. *Nature*, 250, 319–320. <https://doi.org/10.1038/250319a0>
- Kimberley, M.M. (1978) Paleoenvironmental classification of iron formations. *Economic Geology*, 73(2), 215–229. <https://doi.org/10.2113/gsecongeo.73.2.215>
- Kimberley, M.M. (1979) Origin of oolitic iron formations. *Journal of Sedimentary Petrology*, 49, 111–132. <https://doi.org/10.1306/212F76D0-2B24-11D7-8648000102C1865D>

- Kimberley, M.M. (1980) The Paz de Rio oolitic inland-sea iron formation. *Economic Geology*, 75, 97–106. <https://doi.org/10.2113/gsecongeo.75.1.97>
- Kimberley, M.M. (1989) Exhalative origins of iron formations. *Ore Geology Reviews*, 5(1–2), 13–145. [https://doi.org/10.1016/0169-1368\(89\)90003-6](https://doi.org/10.1016/0169-1368(89)90003-6)
- Kimberley, M.M. (1994) Debate about ironstone: has solute supply been surficial weathering, hydrothermal convection, or exhalation of deep fluids? *Terra Nova*, 6(2), 116–132. <https://doi.org/10.1111/j.1365-3121.1994.tb00645.x>
- Kiyokawa, S., Kuratomi, T., Hoshino, T., Goto, S. & Ikehara, M. (2021) Hydrothermal formation of iron-oxyhydroxide chimney mounds in a shallow semi-enclosed bay at Satsuma Iwojima Island, Kagoshima, Japan. *Bulletin*, 133(9–10), 1890–1908. <https://doi.org/10.1130/B35782.1>
- Klaes, B., Thiele-Bruhn, S., Wörner, G., Höschen, C., Mueller, C.W., Marx, P., Arz, H.W., Breuer, S. & Kilian, R. (2023) Iron (hydr) oxide formation in Andosols under extreme climate conditions. *Scientific Reports*, 13(1), 2818. <https://doi.org/10.1038/s41598-023-29727-1>
- Kogbe, C.A. (1978) Origin and composition of the ferruginous oolites and laterites of North-Western Nigeria. *Geologische Rundschau*, 67, 662–674. <https://doi.org/10.1007/BF01802810>
- Krotov, B.P. (1951) Iron source for the formation of sedimentary iron ore deposits. *Dokl. Akad. Nauk SSSR*, 81(5).
- Kutty, T.S. (1971) Two faunal associations from the Maleri Formation of the Pranhita-Godavari Valley. *Geological Society of India*, 12(1), 63–67.
- Kutty, T.S., Jain, S.L. & Roy Chowdhury, T. (1987) Gondwana sequence of the northern Pranhita-Godavari Valley: its stratigraphy and vertebrate faunas. *The Palaeobotanist*, 36, 214–229. <https://doi.org/10.54991/jop.1987.1582>
- Kutty, T.S. & Sengupta, D.P. (1989) The Late Triassic Formations of the Pranhita-Godavari valley and their vertebrate faunal succession—a reappraisal. *Indian Journal of Earth Sciences*, 16(3–4), 189–206.
- Laetsch, T. & Downs, R. (2006) Software for identification and refinement of cell parameters from powder diffraction data of minerals using the RRUFF Project and American Mineralogist Crystal Structure Databases. In 19th General Meeting of the International Mineralogical Association, Kobe, Japan, vol. 23, e28.
- Liu, H., Chen, T., Zou, X., Qing, C. & Frost, R.L. (2013) Effect of Al content on the structure of Al-substituted goethite: a micro-Raman spectroscopic study. *Journal of Raman Spectroscopy*, 44(11), 1609–1614. <https://doi.org/10.1002/jrs.4376>
- Lyell, C.H. (1855) *A manual of elementary geology*, 5th edition. London: John Murray. <https://doi.org/10.5962/bhl.title.50205>
- Maynard, J.B. (1983) *Geochemistry of sedimentary ore deposits*, 1st edition. Heidelberg: Springer. <https://doi.org/10.1007/978-1-4613-9493-8>
- Maynard, J.B. (1986) Geochemistry of oolitic iron ores, an electron microprobe study. *Economic Geology*, 81, 1473–1483. <https://doi.org/10.2113/gsecongeo.81.6.1473>
- McGregor, F., Ramanaidou, E. & Wells, M. (2010) Phanerozoic ooidal ironstone deposits—generation of potential exploration targets. *Applied Earth Science*, 119(1), 60–64. <https://doi.org/10.1179/037174510X12853354810660>
- Mellon, G.B. (1962a) Petrology of Upper cretaceous oolitic iron-rich rocks from northern Alberta. *Economic Geology*, 57, 921–940. <https://doi.org/10.2113/gsecongeo.57.6.921>
- Mellon, G.B. (1962b) Petrology of Cretaceous oolitic iron ore from north western Alberta. *Geological Society of America, Special Publications*, 229–230.
- Mitra, N.D. (1987) Structure and tectonics of Gondwana basins of peninsular India. Coal Resources of India. Dept. of Geology, BHU, 30–41.
- Mitra, N.D. (1994) Tensile Resurgence along fossil sutures: a hypothesis on the evolution of Gondwana Basins of Peninsular India. In Proc. 2nd Symp. on Petroliferous Basins of India. Indian Petroleum Publishers, Dehradun, 55–62.
- Murru, M., Ferrara, C., Matteucci, R., Da Pelo, S., Sarria, E. & Vacca, A. (2011) Pisolithic ferricretes around the Cretaceous–Palaeocene boundary in southern Sardinia (Italy) as palaeoenvironmental proxies. *Comptes Rendus Geoscience*, 343(1), 72–81. <https://doi.org/10.1016/j.crte.2010.12.002>
- Nahon, D., Carozzi, A.V. & Parron, C. (1980) Lateritic weathering as a mechanism for the generation of ferruginous ooids. *Journal of Sedimentary Research*, 50(4), 1287–1298. <https://doi.org/10.1306/212F7BD5-2B24-11D7-8648000102C1865D>
- Naqvi, S.M., Rao, V.D. & Narain, H. (1974) The protocontinental growth of the Indian shield and the antiquity of its rift valleys. *Precambrian Research*, 1(4), 345–398. [https://doi.org/10.1016/0301-9268\(74\)90005-9](https://doi.org/10.1016/0301-9268(74)90005-9)
- Novoselov, K.A., Belogub, E.V., Kotlyarov, V.A., Filippova, K.A. & Sadykov, S.A. (2018) Mineralogical and Geochemical Features of Oolitic Ironstones from the Sinara-Techa Deposit, Kurgan District, Russia. *Geology of Ore Deposits*, 60, 265–276. <https://doi.org/10.1134/S1075701518030066>
- Pascoe, E.H. (1959) *A manual of the geology of India and Burma*, v. 2, 3rd edition. New Delhi: Government of India Publications, pp. 485–1344.
- Pavlov, D.I. (1989) Relation of sedimentary iron and manganese deposits with petroleum basins. *Geol. Rud. Mestorozhd.*, 2, 80–91.
- Pavlov, D.I. (1995) Deposits of oolitic iron ores: supergene and catagenetic—sedimentary types. *Geol. Rud. Mestorozhd.*, 340(4), 518–520.
- Peryt, T.M. (1983) Classification of coated grains. In: *Coated grains*. Berlin Heidelberg: Springer, pp. 3–6. https://doi.org/10.1007/978-3-642-68869-0_1
- Pettijohn, F.J. (1975) *Sedimentary rocks*, Vol. 3. New York: Harper & Row.
- Pirajno, F. (2020) Subaerial hot springs and near-surface hydrothermal mineral systems past and present, and possible extraterrestrial analogues. *Geoscience Frontiers*, 11, 1549–1569. <https://doi.org/10.1016/j.gsf.2020.04.001>
- Prasad, G.V. & Parmar, V. (2020) First Ornithischian and Theropod Dinosaur Teeth from the Middle Jurassic Kota Formation of India: paleobiogeographic relationships. In: Prasad, G.V.R. & Patnaik, R. (Eds.) *Biological consequences of plate tectonics: new perspectives on post-Gondwana break-up—a tribute to Ashok Sahni*. Cham: Springer International Publishing, pp. 1–30. https://doi.org/10.1007/978-3-030-49753-8_1
- Preat, A., El Hassani, A. & Mamet, B. (2008) Iron bacteria in Devonian carbonates (Tafilalt, Anti-Atlas, Morocco). *Facies*, 54, 107–120. <https://doi.org/10.1007/s10347-007-0124-2>
- Preston, L.J., Shuster, J., Fernández-Remolar, D., Banerjee, N.R., Osinski, G.R. & Southam, G. (2011) The preservation and degradation of filamentous bacteria and biomolecules within iron oxide deposits at Rio Tinto, Spain. *Geobiology*, 9(3), 233–249. <https://doi.org/10.1111/j.1472-4669.2011.00275.x>

- Ramajo, J., Aurell, M. & Cepriá, J. (2002) Análisis de facies de la Capa de Oolitos ferruginosos de Arroyofrío en la Sierra de Arcos (Jurásico Cordillera Ibérica Septentrional). *Journal of Iberian Geology*, 28, 45–64.
- Ray, S. & Bandyopadhyay, S. (2003) Late Permian vertebrate community of the Pranhita–Godavari valley, India. *Journal of Asian Earth Sciences*, 21(6), 643–654. [https://doi.org/10.1016/S1367-9120\(02\)00050-0](https://doi.org/10.1016/S1367-9120(02)00050-0)
- Renaut, R.W. & Jones, B. (2011) Hydrothermal environments, terrestrial. In: Reitner, J. & Thiel, V. (Eds.) *Encyclopedia of Geobiology. Encyclopedia of Earth Sciences Series*. Dordrecht: Springer. https://doi.org/10.1007/978-1-4020-9212-1_114
- Renaut, R.W. & Owen, R.B. (2023) Controls on Lacustrine sedimentation in rift settings. In: *The Kenya Rift Lakes: modern and ancient. Syntheses in limnogeology*. Berlin, Heidelberg: Springer. https://doi.org/10.1007/978-3-642-25055-2_22
- Reolid, M. & Abad, I. (2019) The Middle–Upper Jurassic unconformity in the South Iberian palaeomargin (Western Tethys): a history of carbonate platform fragmentation, emersion and subsequent drowning. *Journal of Iberian Geology*, 45, 87–110. <https://doi.org/10.1007/s41513-018-0085-z>
- Reolid, M., Abad, I. & Martín-García, J.M. (2008) Palaeoenvironmental implications of ferruginous deposits related to a Middle–Upper Jurassic discontinuity (Prebetic Zone, Betic Cordillera, southern Spain). *Sedimentary Geology*, 203(1–2), 1–16. <https://doi.org/10.1016/j.sedgeo.2007.10.001>
- Richter, D.K. (1983) Classification of coated grains: discussion. In: *Coated grains*. Berlin Heidelberg: Springer, pp. 7–8. https://doi.org/10.1007/978-3-642-68869-0_2
- Robinson, P.L. (1967) The Indian Gondwana formations—a review. First Symposium on Gondwana Stratigraphy, Mar Del Plata, Argentina. UNESCO, Paris, 201–268.
- Rudra, D.K. (1982) Upper Gondwana stratigraphy and sedimentation in the Pranhita–Godavari valley, India. *Quarterly Journal Geological, Mining and Metallurgical Society (India)*, 54, 56–79.
- Rudra, D.K. & Maulik, P.K. (1994) Lower Jurassic Kota Limestone of India. *Global Geological Record of Lake Basins*, 1, 185–191.
- Sarkar, S. & Chaudhuri, A.K. (1992) Trace fossils in Middle to Late Triassic fluvial redbeds, Pranhita–Godavari Valley, south India. *Ichnos: An International Journal of Plant & Animal*, 2(1), 7–19. <https://doi.org/10.1080/10420949209380071>
- Scholle, P.A. & Ulmer-Scholle, D.S. (2003) A color guide to the petrography of carbonate rocks: grains, textures, porosity, diagenesis. *AAPG Memoir*, 77(Vol. 77), AAPG. <https://doi.org/10.1306/M77973>
- Schulze, D.G. (1984) The influence of aluminum on iron oxides. VIII. Unit-cell dimensions of Al-substituted goethites and estimation of Al from them. *Clays and Clay Minerals*, 32(1), 36–44. <https://doi.org/10.1346/CCMN.1984.0320105>
- Schwertmann, U. & Murad, E. (1983) Effect of pH on the Formation of Goethite and Hematite from Ferrihydrite. *Clays and Clay Minerals*, 31(4), 277–284. <https://doi.org/10.1346/CCMN.1983.0310405>
- Schwertmann, U. & Taylor, R.M. (1989) Iron oxides. In: Dixon, J.B. & Weed, S.B. (Eds.) *Minerals in soil environments*, 2nd edition. Madison, WI: Soil Science Society of America, pp. 379–427. <https://doi.org/10.2136/sssabookser1.2ed.c8>
- Sengupta, S. (1970) Gondwana Sedimentation around Bheemaram (Bhimaram), Pranhita–Godavari Valley, India. *Journal of Sedimentary Petrology*, 40(1), 140–170. <https://doi.org/10.1306/74d71f0a-2b21-11d7-8648000102c1865d>
- Shanks, W.P., III, Koski, R.A., Mosier, D.L., Schulz, K.J., Morgan, L.A., Slack, J.F., Ridley, W.I., Dusel-Bacon, C., Seal, R.R., II & Piatak, N.M. (2012) Volcanogenic massive sulfide occurrence model: chapter C in mineral deposit models for resource assessment (No. 2010-5070-C). US Geological Survey <https://doi.org/10.3133/sir20105070C>
- Siehl, A. & Thein, J. (1978) Geochemische Trends in der Minette (Jura, Luxemburg/Lothringen). *Geologische Rundschau*, 67, 1052–1077. <https://doi.org/10.1007/BF01983254>
- Siehl, A. & Thein, J. (1989) Minette-type ironstones. *Geological Society, London, Special Publications*, 46(1), 175–193. <https://doi.org/10.1144/GSL.SP.1989.046.01.16>
- Smith, A.J., Beukes, N.J., Gutzmer, J., Johnson, C.M., Czaja, A.D., Nhleko, N., De Beer, F., Hoffman, J.W. & Awramik, S.M. (2020) Life on a Mesoproterozoic marine shelf—insights from the world’s oldest known granular iron formation. *Scientific Reports*, 10(1), 10519. <https://doi.org/10.1038/s41598-020-66805-0>
- Sorby, H.C. (1856) On the origin of the Cleveland Hill ironstone. *Proceedings of the Geological and Polytechnic Society of the West Riding of Yorkshire*, 3, 457–461. <https://doi.org/10.1144/pygs.3.457>
- Soussi, M. & M’rabet, A. (1991) Les Faciès à oolites ferrugineuses (oolitic ironstones) du Jurassique moyen de l’Axe Nord-Sud (Tunisie centrale): Caractéristiques et significations. *Notes du Service géologique*, 57, 71–85.
- Stanton, M.R., Yager, D.B., Fey, D.L. & Wright, W.G. (2007) Formation and geochemical significance of iron bog deposits. US Geological Survey professional paper 1651.
- Stoops, G. & Marcelino, V. (2018) Lateritic and bauxitic materials. In: *Interpretation of micromorphological features of soils and regoliths*. Elsevier, pp. 691–720. <https://doi.org/10.1016/B978-0-444-63522-8.00024-3>
- Sturesson, U. (2003) Lower Palaeozoic iron oolites and volcanism from a Baltoscandian perspective. *Sedimentary Geology*, 159(3–4), 241–256. [https://doi.org/10.1016/S0037-0738\(02\)00330-5](https://doi.org/10.1016/S0037-0738(02)00330-5)
- Sturesson, U., Heikoop, J.M. & Risk, M.J. (2000) Modern and Palaeozoic iron ooids—a similar volcanic origin. *Sedimentary Geology*, 136(1–2), 137–146. [https://doi.org/10.1016/S0037-0738\(00\)00091-9](https://doi.org/10.1016/S0037-0738(00)00091-9)
- Taylor, K.G., Simo, J.A., Yocum, D. & Leckie, D.A. (2002) Stratigraphic significance of ooidal ironstones from the Cretaceous western interior seaway: the Peace River Formation, Alberta, Canada, and the Castlegate Sandstone, Utah, USA. *Journal of Sedimentary Research*, 72(2), 316–327. <https://doi.org/10.1306/060801720316>
- Tazaki, K., Okuno, M., Furumoto, M. & Watanabe, H. (2006) Biomineralization of pisolites in hot springs. *Materials Science and Engineering: C*, 26(4), 617–623. <https://doi.org/10.1016/j.msec.2005.07.022>
- Thorne, R., Anand, R. & Suvorova, A. (2014) The formation of fluvio-lacustrine ferruginous pisolites in the extensive palaeochannels of the Yilgarn Craton, Western Australia. *Sedimentary Geology*, 313, 32–44. <https://doi.org/10.1016/j.sedgeo.2014.08.004>
- Tucker, M.E. & Wright, V.P. (1990) *Carbonate sedimentology*. Boston: Blackwell Scientific Publications, p. 482.
- Van Houten, F.B. (1992) Review of Cenozoic ooidal ironstones. *Sedimentary Geology*, 78(1–2), 101–110. [https://doi.org/10.1016/0037-0738\(92\)90115-8](https://doi.org/10.1016/0037-0738(92)90115-8)
- Van Houten, F.B. & Purucker, M.E. (1984) Glauconitic peloids and chamositic ooids – favorable factors, constraints, and

- problems. *Earth-Science Reviews*, 20(3), 211–243. [https://doi.org/10.1016/0012-8252\(84\)90002-3](https://doi.org/10.1016/0012-8252(84)90002-3)
- Veevers, J.J. & Tewari, R.C. (1995) Gondwana master basin of peninsular India between Tethys and the interior of the Gondwanaland province of Pangea. *Memoir—Geological Society of America*, 187, 1–73.
- Verplanck, P.L., Yager, D.B., Church, S.E. & Stanton, M.R. (2007) Ferricrete classification, morphology, distribution, and ^{14}C age constraints. In: Church, S.E., von Guerard, P. & Finger, S.E. (Eds.), *Integrated investigations of environmental effects of historical mining in the Animas River watershed, San Juan County, Colorado*. U.S Geological Survey Professional Paper 1651, 721–744.
- Wolf, K.H. (1960) Simplified limestone classification. *AAPG Bulletin*, 44(8), 1414–1416.
- Young, T.P. (1989) Phanerozoic ironstones: an introduction and review. *Geological Society, London, Special Publications*, 46(1), ix–xxv. <https://doi.org/10.1144/GSL.SP.1989.046.01.02>
- Young, T.P. & Taylor, W.E.G. (Eds) (1989) Phanerozoic ironstones. *Geological Society Special Publication*, 46, xxv+251.
- Zúñiga, F., Dec, D., Valle, S.R., Thiers, O., Paulino, L., Martínez, O., Seguel, O., Casanova, M., Pino, M., Horn, R. & Dörner, J. (2019) The waterlogged volcanic ash soils of southern Chile. A review of the “Ñadi” soils. *Catena*, 173, 99–113. <https://doi.org/10.1016/j.catena.2018.10.003>

How to cite this article: Datta, S., Sain, A., Goswami, S., Ghosh, P. & Arenas Abad, C. (2024) Origin of ferruginous coated grains in the Lower Jurassic palustrine limestones of the Pranhita–Godavari Basin, India. *The Depositional Record*, 00, 1–26. Available from: <https://doi.org/10.1002/dep2.285>